

A high-throughput *ab initio* review of platinum-group alloy systems

Gus L.W. Hart,¹ Stefano Curtarolo,^{2,*} Thaddeus B. Massalski,³ and Ohad Levy²

¹*Department of Physics and Astronomy, Brigham Young University, Provo UT 84602, USA*

²*Center for Materials Genomics and Department of Mechanical Engineering and Materials Science, Duke University, Durham NC 27708, USA*

³*Materials Science, Engineering and Physics, Carnegie Mellon University, Pittsburgh, PA 15213, USA*

We report a comprehensive study of the binary systems of the platinum group metals with the transition metals, using high-throughput first-principles calculations. These computations predict stability of new compounds in 37 binary systems where no compounds have been reported in the literature experimentally, and a few dozen of as yet unreported compounds in additional systems. Our calculations also identify stable structures at compound compositions that have been previously reported without detailed structural data and indicate that some experimentally reported compounds may actually be unstable at low temperatures. With these results we construct enhanced structure maps for the binary alloys of platinum group metals. These are much more complete, systematic and predictive than those based on empirical results alone.

I. INTRODUCTION

The platinum group metals (PGMs), osmium, iridium, ruthenium, rhodium, platinum and palladium, are immensely important in numerous technologies, but the experimental and computational data on their binary alloys still contains many gaps. Interest in PGMs is driven by their essential role in a wide variety of industrial applications, which is at odds with their high cost. The primary application of PGMs is in catalysis, where they are core ingredients in the chemical, petroleum and automotive industries. They also extensively appear as alloying components in aeronautics and electronics applications. The use of platinum alloys in the jewelry industry also accounts for a sizeable fraction of its worldwide consumption, about 30% over the last decade [1]. The importance and high cost of PGMs motivate numerous efforts directed at more effective usage, or at the development of less-expensive alloy substitutes. Despite these efforts, there are still sizeable gaps in the knowledge about the basic properties of PGMs and their alloys; many of the possible alloy compositions have not yet been studied and there is a considerable difficulty in application of thermodynamic experiments because they often require high temperatures or pressures and very long equilibration processes.

The possibility of predicting the existence of ordered structures in alloy systems from their starting components is a major challenge of current materials research. Empirical methods use experimental data to construct structure maps and make predictions based on clustering of simple physical parameters. Their usefulness depends on the availability of reliable data over the entire parameter space of components and stoichiometries. Advances in first-principles methods for the calculation of materials properties open the possibility to complement the experimental data by computational results. Indeed many recent studies present such calculations of PGM alloy structures [2–25]. However, most of these studies consider a limited

number of structures, at just a few stoichiometries of a single binary system or a few systems [3–17]. Some cluster expansion studies of specific binary systems include a larger set of structures, but limited to a single lattice type (usually, fcc) [18–23]. Realizing the potential of first-principles calculations to complement the lacking, or only partial, empirical data requires high-throughput computational screening of large sets of materials, with structures spanning all lattice types and including, in addition, a considerable number of off-lattice structures [2, 26–28]. Such large scale screenings can be used to construct low-temperatures binary phase diagrams. They provide insights into trends in alloy properties and indicate the possible existence of hitherto unobserved compounds [27]. A few previous studies implemented this approach to binary systems of specific metals, hafnium, rhenium, rhodium, ruthenium and technetium [24, 25, 29–31].

The capability to identify new phases is key to tuning the catalytic properties of PGM alloys and their utilization in new applications, or as reduced-cost or higher-activity substitutes in current applications. Even predicted phases that are difficult to access kinetically in the bulk may be exhibited in nanophase alloys [32] and could be used to increase the efficiency or the lifetimes of PGM catalysts. Given the potential payoff of uncovering such phases, we have undertaken a thorough examination of PGM binary phases with the transition metals, using the first-principles high-throughput (HT) framework AFLOW [33, 34]. We find new potentially stable PGM phases in many binary systems and, comparing experimental data with our predictions, we construct enhanced Pettifor-type maps that demonstrate new ordering trends and compound forming possibilities in these alloys.

II. METHODS

Computations of the low-temperature stability of the PGM-transition metal systems were carried out using the HT framework AFLOW [33, 34]. For each of the 153 binary systems studied, we calculated the energies of more than 250 structures, including all the crystal structures reported for the system in the phase diagram literature [35, 36]

*E-mail address: stefano@duke.edu

and additional structures from the AFLOWLIB database of prototypes and hypothetical hcp-, bcc- and fcc-derivative superstructures [33]. A complete list of structures examined for each binary system can be found on the on-line repository, www.afflowlib.org [34]. The low temperature phase diagram of a system is constructed as the minimum formation enthalpy convex hull from these candidate structures, identifying the ordering trends in each alloy system and indicating possible existence of previously unknown compounds. It should be noted that there is no guarantee that the true groundstates of a system will be found among the common experimentally observed structures or among small-unit-cell derivative structures. However, even if it is impossible to rule out the existence of additional unexpected groundstates, this protocol (searching many enumerated derivative structures [37] and exhaustively exploring experimentally reported ones) is expected to give a reasonable balance between high-throughput speed and scientific accuracy to determine miscibility (or lack thereof) in these alloys. In Ref. [2], it was shown that the probability of reproducing the correct ground state, if well defined and not ambiguous, is $\eta_C^* \sim 96.7\%$ [“reliability of the method,” Eq. (3)].

The calculations of the structure energies were performed with the VASP software [38] with projector augmented waves pseudopotentials [39] and the exchange-correlation functionals parameterized by Perdew, Burke and Ernzerhof for the generalized gradient approximation [40]. The energies were calculated at zero temperature and pressure, with spin polarization and without zero-point motion or lattice vibrations. All crystal structures were fully relaxed (cell volume and shape and the basis atom coordinates inside the cell). Numerical convergence to about 1 meV/atom was ensured by a high energy cutoff (30% higher than the maximum cutoff of both potentials) and a 6000 \mathbf{k} -point, or higher, Monkhorst-Pack mesh [41].

The presented work comprises 38,954 calculations, performed by using 1.82 million CPU/hours on 2013 Intel Xeon E5 cores at 2.2GHz. It was carried out by extending the pre-existing AFLOWLIB structure database [34] with additional calculations characterizing PGM alloys. Detailed information about all the examined structures can be found on the on-line repository, www.afflowlib.org [34], including input/output files, calculation parameters, geometry of the structures, energies and formation energies. In addition, the reader can prepare phase diagrams (as in figs. 5 to 12) linked to the appropriate structure URL locations.

The analysis of formation enthalpy is, by itself, insufficient to compare alloy stability at different concentrations and their resilience toward high-temperature disorder. The formation enthalpy, $\Delta H(A_x B_{1-x}) \equiv H(A_x B_{1-x}) - xH(A) - (1-x)H(B)$, represents the ordering-strength of a mixture $A_x B_{1-x}$ against decomposition into its pure constituents at the appropriate proportion xA and $(1-x)B$ (ΔH is negative for compound forming systems). However, it does not contain information about its resilience against disorder, which is captured by the entropy of the system. To quantify this resilience we define the *entropic*

temperature

$$T_s \equiv \max_i \left[\frac{\Delta H(A_{x_i} B_{1-x_i})}{k_B [x_i \log(x_i) + (1-x_i) \log(1-x_i)]} \right], \quad (1)$$

where i counts all the stable compounds identified in the AB binary system by the *ab initio* calculations, and the sign is chosen so that a positive temperature is needed for competing against compound stability. This definition assumes an ideal scenario [28] where the entropy is $S[\{x_i\}] = -k_B \sum_i x_i \log(x_i)$. This first approximation should be considered as indicative of a trend (see Fig. 1 of Ref. [28] and Fig. 1 below), which might be modified somewhat by a system specific thorough analysis of the disorder. T_s is a concentration-maximized formation enthalpy weighted by the inverse of its entropic contribution. It represents the deviation of a system convex-hull from the purely entropic free-energy hull, $-TS(x)$, and hence the ability of its ordered phases to resist the deterioration into a temperature-driven, entropically-promoted, disordered binary mixture.

III. HIGH-THROUGHPUT RESULTS

We examined the 153 binary systems containing a PGM and a transition metal, including the PGM-PGM pairs, (see Fig. 1). An exhaustive comparison of experimental and computational groundstates is given in tables I to VI. Convex hulls for systems which exhibit compounds are shown in the Appendix (figs. 5 to 12). These results uncover 37 alloy systems reported as non-compound forming in the experimental literature, but predicted computationally to have low-temperature stable compounds. Dozens of new compounds are also predicted in systems known to be compound forming.

The top panel of Fig. 1 gives a broad overview of the comparison of experiment and computation. Green circles (dark gray) indicate systems where experiment and computation agree that the system is compound forming. Light gray circles indicate agreement that the system is not compound-forming. The elements along the axes of this diagram are listed according to their Pettifor χ parameter [42, 43], leading, as expected, to compound-forming and non-compound forming systems separating rather cleanly into different broad regions of the diagram. Most of the compound-forming systems congregate in a large cluster on the left half of the diagram, and in a second smaller cluster at the lower right corner.

The systems for which computation predicts compounds but experiment does not report any are marked by red squares. As is clear in the top panel of Fig. 1, these systems, which harbor potential new phases, occur near the boundary between the compound-forming and non-compound-forming regions of the diagram. They also fill in several isolated spots where experiment reports no compounds in the compound-forming region (e.g., Pd-W, Ag-Pd), and bridge the gap between the large cluster of compound-forming systems, on the left side of the panel, and the small island of such systems at its center. The

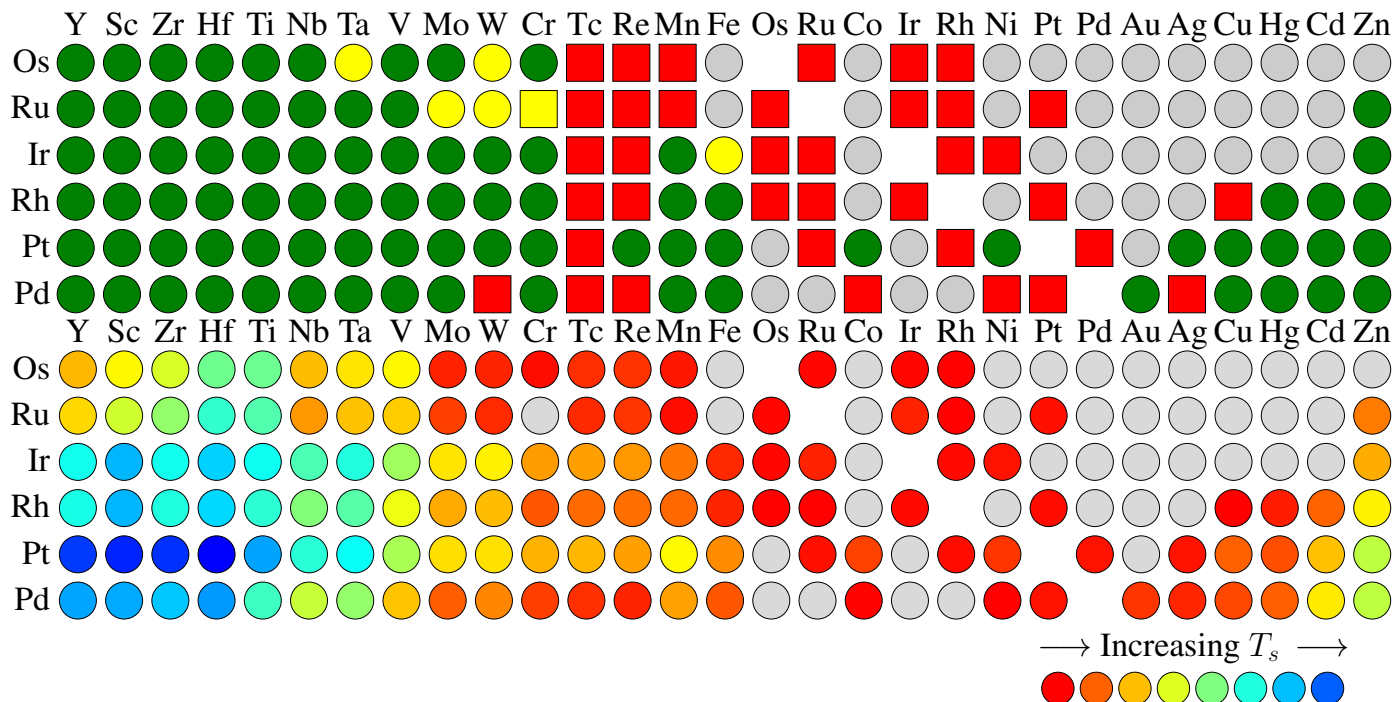


FIG. 1: Top panel: Compound-forming vs. non-compound-forming systems as determined by experiment and computation. Circles indicate agreement between experiment and computation, green for compound-forming systems, gray for non-compound-forming systems. Yellow circles indicate systems reported in experiment to have disordered phases, for which low-energy compounds were found in this work. Ru-Cr is the only system (yellow square) experimentally reported to include a disordered phase where no low-temperature stable compounds were found. Red squares mark systems for which low-temperature compounds are found in computation but no compounds are reported in experiment. Bottom panel: T_s for the binary systems in this work. Colors: from red (lowest T_s) to blue (highest T_s).

computations also predict ordered structures in most systems reported only with disordered phases (yellow circles in top panel of Fig. 1). Two disordered phases, σ and χ , turn up in the experimental literature on PGM alloys. In the HT search, we included all ordered realizations of these phases (the prototypes $\text{Al}_{12}\text{Mg}_{17}$ and $\text{Re}_{24}\text{Ti}_5$ are ordered versions of the χ phase and the σ phase has 32 ordered realizations, denoted by σ_{XXXXX} where $X = A, B$). In most of these systems we find one of these corresponding ordered structures to be stable. The only exception is the Cr-Ru system, where the lowest lying ordered phase is found just 4 meV/atom above the elements tie-line (yellow square in Fig. 1). These results thus identify the low temperature ordered compounds that underly the reported disordered phases. The calculated compound-forming regions are considerably more extensive than reported by the available experimental data, identifying potential new systems for materials engineering.

The bottom panel of Fig. 1 ranks systems by their estimated entropic temperature T_s . Essentially, the (top panel) map, incorporating the computational data, corresponds to what would be observed at low temperatures, assuming thermodynamic equilibrium, whereas a map with only experimental data reports systems as compound-forming when reaching thermodynamic equilibrium is presumably easier. That is not to say, however, that the predicted phases will necessarily be difficult to synthesize—some of the systems where the T_s value is small have

been experimentally observed to be compound-forming (e.g., Cr-Pd, Au-Pd, Ag-Pt, Hg-Rh and Co-Pt). T_s decreases gradually as we move from the centers of the compound-forming clusters towards their edges. Most systems with low T_s are adjacent to the remaining non-compound-forming region. This leads to a qualitative picture of compound stability against disorder which is correlated with the position of a system within the compound-forming cluster, and with larger clusters centered at systems with more stable structures.

It is instructive to note that many obscure and large unit cell structures that are reported in the experimental literature are recovered in the HT search. For example, compounds of prototypes such as $\text{Mg}_{44}\text{Rh}_7$, $\text{Ru}_{25}\text{Y}_{44}$, $\text{Ir}_4\text{Sc}_{11}$, $\text{Rh}_{13}\text{Sc}_{57}$ from the experimental literature, nearly always turn up as ground states, or very close to the convex hull, in the HT search as well. This is strong evidence that the first-principles HT approach is robust and has the necessary accuracy to extend the PGM data where experimental results are sparse or difficult to obtain. Also of interest is the appearance of some rare prototypes in systems similar to those in which they were identified experimentally. For example, the prototype Pd_3Ti_2 , reported only in the Pd-Ti system [36], also emerges as a calculated groundstate in the closely related systems Hf-Pd and Pt-Ti. In Hf-Pt, it appears as marginally stable, at 3meV/atom above the convex hull, in agreement with a very recent experimental study that identified the previously incorrectly character-

TABLE I: Compounds observed in experiments (“Exper.”) or predicted by *ab initio* calculations (“Calc.”) in **Osmium** binary alloys (structure prototype in parentheses, multiple entries denote different reported structures, in the experiments, or degenerate structures, in the calculations). “-” denotes no compounds. The superscript “*” denotes unobserved prototypes found in calculations [2, 13, 25, 27, 29, 31]. ΔH are the formation enthalpies from the present study. The energy difference between reported and calculated structures or between the reported structure (unstable in the calculation) and a two-phase tie-line is indicated in brackets “⟨.⟩”.

	Compounds		ΔH meV/at.		Compounds		ΔH meV/at.
	Exper.[35, 36]	Calc.			Exper.[35, 36]	Calc.	
Y	Os ₂ Y(C14)	Os ₂ Y(C14)	-304	W	Os ₃ W(D0 ₁₉)	-56	
	OsY ₃ (D0 ₁₁)	OsY ₃ (D0 ₁₁)	-239		Os _{0.3} W _{0.7} (σ)		
Sc	Os ₂ Sc(C14)	Os ₂ Sc(C14)	-390	Cr	Cr ₃ Os(A15)	⟨18⟩	
		OsSc ₂ (fcc ^[001] _{AB2})	-400		CrOs ₃ (D0 ₁₉)	-22	
	Os ₄ Sc ₁₁ (Ir ₄ Sc ₁₁)	Os ₄ Sc ₁₁ (Ir ₄ Sc ₁₁)	-372		CrOs ₅ (Hf ₅ Sc*)	-19	
	Os ₇ Sc ₄₄ (Mg ₄₄ Rh ₇)	Os ₇ Sc ₄₄ (Mg ₄₄ Rh ₇)	-197	Tc	-	Os ₃ Tc(D0 ₁₉)	-71
Zr	Os ₂ Zr(C14)	Os ₂ Zr(C14)	-388			OsTc(B19)	-83
	OsZr(B2)	OsZr(B2)	-524			OsTc ₃ (D0 ₁₉)	-57
	Os ₄ Zr ₁₁ (Ir ₄ Sc ₁₁)	Os ₄ Zr ₁₁ (Ir ₄ Sc ₁₁)	-29	Re	-	Os ₃ Re(D0 ₁₉)	-78
	Os ₁₇ Zr ₅₄ (Hf ₅₄ Os ₁₇)		⟨8⟩			OsRe(B19)	-89
	OsZr ₄ (D1 _a)	-220			OsRe ₂ (Sc ₂ Zr*)	-68	
Hf	Hf ₅₄ Os ₁₇ (Hf ₅₄ Os ₁₇)		⟨20⟩			OsRe ₃ (Re ₃ Ru*)	-56
	Hf ₂ Os(NiTi ₂)		⟨44⟩	Mn	-	MnOs(B19)	-42
	HfOs(B2)	HfOs(B2)	-709			MnOs ₃ (D0 ₁₉)	-36
	HfOs ₂ (C14)		⟨66⟩	Fe	-	-	
Ti	OsTi(B2)	OsTi(B2)	-714	Os	reference		
		OsTi ₂ (C49)	-515	Ru	-	Os ₃ Ru(D0 _a)	-9
		OsTi ₃ (Mo ₃ Ti*)	-403			OsRu(B19)	-15
					OsRu ₃ (D0 _a)	-11	
Nb		Nb ₅ Os(HfPd ₅)	-200			OsRu ₅ (Hf ₅ Sc*)	-9
	Nb ₃ Os(A15)	Nb ₃ Os(A15)	-275	Co	-	-	
	Nb _{0.6} Os _{0.4} (σ)	Nb ₂₀ Os ₁₀ ($\sigma_{B A A B A}$)	-274	Ir	-	Ir ₈ Os(Pt ₈ Ti)	-8
	Nb _{0.4} Os _{0.6} (χ)	Nb ₁₂ Os ₁₇ (Al ₁₂ Mg ₁₇)	-247			IrOs ₅ (Hf ₅ Sc*)	-7
	NbOs ₃ (D0 ₂₄)	-115					
Ta		Os ₂ Ta(Ga ₂ Hf)	-205	Rh	-	OsRh(RhRu*)	-8
	Os _{0.5} Ta _{0.5} (χ)	Os ₁₂ Ta ₁₇ (Al ₁₂ Mg ₁₇)	-313	Ni	-	-	
	Os _{0.3} Ta _{0.7} (σ)	Os ₁₀ Ta ₂₀ ($\sigma_{A B B A B}$)	-335	Pt	-	-	
		OsTa ₃ (A15)	-330	Pd	-	-	
V		Os ₃ V(Re ₃ Ru*)	-150	Au	-	-	
		Os ₃ V ₅ (Ga ₃ Pt ₅)	-350	Ag	-	-	
		OsV ₂ (C11 _b)	-354	Cu	-	-	
	OsV ₃ (A15)	OsV ₃ (D0 ₃)	-361⟨21⟩	Hg	-	-	
		OsV ₅ (Mo ₅ Ti*)	-253	Cd	-	-	
Mo	Mo ₃ Os(A15)		⟨29⟩	Zn	-	-	
	Mo _{0.65} Os _{0.35} (σ)						
		MoOs ₃ (D0 ₁₉)	-52				

ized structure of a Hf₂Pt₃ phase [46].

In the systems we examined, there are nearly 50 phases reported in the experimental phase diagrams for which the crystal structure of the phase is not known. In one half of these cases, the HT calculations identify stable structures for these unknown phases. For the other half of these unknown structures, our calculations find no stable compounds at the reported concentration, but stable compounds at other concentrations. The reported phases (sans structural information) may, therefore, be due to

phases that decompose at low temperatures or may merely represent samples that were kinetically inhibited and unable to settle into their stable phases during the time frame of the experiments.

The prototype database included in this study comprise both experimentally-reported structures as well as hypothetical structures constructed combinatorially from derivative supercells of fcc, bcc, and hcp lattices [37, 47]. Occasionally these derivative superstructures are predicted to be ground states by the first-principles calcu-

TABLE II: Compounds in **Ruthenium** binary alloys. (Unkn.) denotes an unknown structure. All other symbols are as in Table I.

	Compounds		ΔH meV/at.		Compounds		ΔH meV/at.
	Exper.[35, 36]	Calc.			Exper.[35, 36]	Calc.	
Y	Ru ₂ Y(C14)	Ru ₂ Y(C14)	-313	Mo	Mo _{0.6} Ru _{0.4} (σ)	Mo ₁₄ Ru ₁₆ (σ_{AABAB})	-116
	Ru ₂ Y ₃ (Er ₃ Ru ₂)		(79)	W	Ru _{0.4} W _{0.6} (σ)	Ru ₃ W(D0 ₁₉)	-65
	Ru ₂₅ Y ₄₄ (Ru ₂₅ Y ₄₄)	Ru ₂₅ Y ₄₄ (Ru ₂₅ Y ₄₄)	-342	Cr	Cr _{0.7} Ru _{0.3} (σ)	-	
	Ru ₂ Y ₅ (C ₂ Mn ₅)	Ru ₂ Y ₅ (C ₂ Mn ₅)	-334	Tc	-	Ru ₃ Tc(D0 ₁₉)	-63
	RuY ₃ (D0 ₁₁)	RuY ₃ (D0 ₁₁)	-307			RuTc(B19)	-73
Sc	Ru ₂ Sc(C14)	Ru ₂ Sc(C14)	-389			RuTc ₃ (D0 ₁₉)	-47
	RuSc(B2)	RuSc(B2)	-540			RuTc ₅ (RuTc ₅ [*])	-32
	Ru ₃ Sc ₅ (D8 ₈)		(42)	Re	-	Re ₃ Ru(Re ₃ Ru [*])	-53
	RuSc ₂ (NiTi ₂)	RuSc ₂ (C11 _b)	-484(84)			ReRu(B19)	-86
	Ru ₄ Sc ₁₁ (Ir ₄ Sc ₁₁)	Ru ₄ Sc ₁₁ (Ir ₄ Sc ₁₁)	-405			ReRu ₃ (D0 ₁₉)	-80
	Ru ₁₃ Sc ₅₇ (Rh ₁₃ Sc ₅₇)		(10)	Mn	-	Mn ₂₄ Ru ₅ (Re ₂₄ Ti ₅)	-18
	Ru ₇ Sc ₄₄ (Mg ₄₄ Rh ₇)	Ru ₇ Sc ₄₄ (Mg ₄₄ Rh ₇)	-226	Fe	-	-	
	Zr	RuZr(B2)	RuZr(B2)	-644	Os	-	Os ₃ Ru(D0 _a)
Hf	HfRu(B2)	HfRu(B2)	-819			OsRu(B19)	-15
	HfRu ₂ (Unkn.)					OsRu ₃ (D0 _a)	-11
Ti	RuTi(B2)	RuTi(B2)	-763			OsRu ₅ (Hf ₅ Sc [*])	-9
		RuTi ₂ (C49)	-532	Ru	Reference		
		RuTi ₃ (Mo ₃ Ti [*])	-401	Co	-	-	
Nb		Nb ₈ Ru(Pt ₈ Ti)	-117	Ir	-	Ir ₈ Ru(Pt ₈ Ti)	-20
		Nb ₅ Ru(Nb ₅ Ru [*])	-172			Ir ₃ Ru(L1 ₂)	-34
		Nb ₃ Ru(L6 ₀)	-222			IrRu(B19)	-49
		Nb ₅ Ru ₃ (Ga ₃ Pt ₅)	-249			IrRu ₂ (Ir ₂ Tc [*])	-54
	NbRu(Unkn.)					IrRu ₃ (D0 ₁₉)	-53
		Nb ₃ Ru ₅ (Ga ₃ Pt ₅)	-240			IrRu ₅ (Hf ₅ Sc [*])	-37
Ta		NbRu ₃ (L1 ₂)	(8)	Rh	-	Rh ₈ Ru(Pt ₈ Ti)	-2
	Ru ₅ Ta ₃ (Unkn.)	Ru ₅ Ta ₃ (Ga ₃ Pt ₅)	-332			RhRu(RhRu [*])	-8
	RuTa(Unkn.)					RhRu ₂ (RhRu ₂ [*])	-6
		Ru ₃ Ta ₅ (Ga ₃ Pt ₅)	-313			RhRu ₅ (RhRu ₅ [*])	-3
		RuTa ₃ (fcc _{AB3} ^[001])	-281	Ni	-	-	
V		RuTa ₅ (Nb ₅ Ru [*])	-207	Pt	-	PtRu(CdTi)	-33
		Ru ₃ V(Re ₃ Ru [*])	-145	Pd	-	-	
		Ru ₂ V(C37)	-192	Au	-	-	
	RuV(B11)		(28)	Ag	-	-	
		Ru ₃ V ₅ (Ga ₃ Pt ₅)	-313	Cu	-	-	
		RuV ₂ (C11 _b)	-321	Hg	-	-	
		RuV ₃ (Mo ₃ Ti [*])	-296	Cd	-	-	
		RuV ₄ (D1 _a)	-262	Zn		RuZn ₃ (L1 ₂)	-150
	RuV ₅ (Nb ₅ Ru [*])	-230		RuZn ₆ (RuZn ₆)	RuZn ₆ (RuZn ₆)	-132	
	RuV ₈ (Pt ₈ Ti)	-154					

lations. In this work, we find compounds with 5 of these new structures, for which no prototype is known and no *Strukturbericht* designation have been given. These new prototypes are marked by a † in tables I to VI and their crystallographic parameters are given in Table VII. We also find a few other compounds with unobserved prototypes (marked by a * in tables I to VI) previously uncovered in related HT studies [2, 13, 25, 27, 29, 31].

IV. STRUCTURE MAPS

Empirical structure maps present available experimental data in ways that highlight similarities in materials behavior in alloy systems. Their arrangement principles usually depend on simple parameters, e.g., atomic number, atomic radius, electronegativity, ionization energy, melting temperature or enthalpy. Several well-known classification methods include Hume-Rothery rules

TABLE III: Compounds in **Iridium** binary alloys. The superscript “§” denotes relaxation of one prototype into another and a “†” denotes new prototypes described in Table VII. The other symbols are as in Table II.

	Compounds		ΔH meV/at.		Compounds		ΔH meV/at.
	Exper.[35, 36]	Calc.			Exper.[35, 36]	Calc.	
Y	Ir ₃ Y(PuNi ₃)		(21)	W	Ir ₈ W(Pt ₈ Ti)	-157	
	Ir ₂ Y(C15)	Ir ₂ Y(C15)	-803		Ir ₃ W(D0 ₁₉)	Ir ₃ W(D0 ₁₉)	-350
	IrY(B2)	IrY(B2)	-787			Ir ₂ W(C37)	-352
	Ir ₂ Y ₃ (Rh ₂ Y ₃)		(12)		IrW(B19)	IrW(B19)	-300
	Ir ₃ Y ₅ (Pu ₅ Rh ₃)	Ir ₃ Y ₅ (Pu ₅ Rh ₃)	-772	Cr	Cr ₃ Ir(A15)	(48)	
	Ir ₂ Y ₅ (C ₂ Mn ₅)	Ir ₂ Y ₅ (C ₂ Mn ₅)	-640		Cr _{0.5} Ir _{0.5} (Mg)	CrIr(B19)	-239
	IrY ₃ (D0 ₁₁)	IrY ₃ (D0 ₁₁)	-564			CrIr ₂ (C37)	-233
Sc		Ir ₇ Sc(CuPt ₇)	-352		CrIr ₃ (D0 ₁₉)	-228	
	Ir ₃ Sc(L1 ₂)		(7)	Tc	-	Ir ₈ Tc(Pt ₈ Ti)	-89
	Ir ₂ Sc(C15)	Ir ₂ Sc(C14)	-783(35)			Ir ₂ Tc(Ir ₂ Tc [*])	-224
	IrSc(B2)	IrSc(B2)	-1032			IrTc(B19)	-287
	IrSc ₂ (NiTi ₂)		(26)			IrTc ₃ (D0 ₁₉)	-217
	Ir ₄ Sc ₁₁ (Ir ₄ Sc ₁₁)	Ir ₄ Sc ₁₁ (Ir ₄ Sc ₁₁)	-686	Re	-	Ir ₈ Re(Pt ₈ Ti)	-94
	Ir ₁₃ Sc ₅₇ (Rh ₁₃ Sc ₅₇)		(2)			Ir ₂ Re(Ir ₂ Tc [*])	-227
	Ir ₇ Sc ₄₄ (Mg ₄₄ Rh ₇)	Ir ₇ Sc ₄₄ (Mg ₄₄ Rh ₇)	-369			IrRe(B19)	-274
Zr	Ir ₃ Zr(L1 ₂)	Ir ₃ Zr(L1 ₂)	-709		IrRe ₃ (D0 ₁₉)	-209	
	Ir ₂ Zr(C15)	Ir ₂ Zr(Ga ₂ Hf)	-766(87)	Mn		Ir ₃ Mn(L1 ₂)	-173
	IrZr(NiTi)	IrZr(NiTi)	-830			IrMn(B19)	-204(58)
	Ir ₃ Zr ₅ (Ir ₃ Zr ₅)	Ir ₃ Zr ₅ (Ir ₃ Zr ₅)	-732			IrMn ₂ (C37)	-175
	IrZr ₂ (C16)	IrZr ₂ (C37)	-668(13)		IrMn ₃ (L1 ₂)	IrMn ₃ (L6 ₀)	-156(108)
	IrZr ₃ (SV ₃)	IrZr ₃ (SV ₃)	-519	Fe		Fe ₃ Ir(L6 ₀)	-44
Hf	Hf ₂ Ir(NiTi ₂)	Hf ₂ Ir(C37)	-750(31)			Fe _{0.6} Ir _{0.4} (Mg)	FeIr(NbP)
	Hf ₅ Ir ₃ (D8 ₈ / Ir ₅ Zr ₃)	Hf ₅ Ir ₃ (Ir ₅ Zr ₃)	-814(14)			FeIr ₃ (D0 ₂₂)	-63
	HfIr (Unkn.)	HfIr(B27)	-949	Os	-	Ir ₈ Os(Pt ₈ Ti)	-8
		HfIr ₂ (Ga ₂ Hf)	-872			IrOs ₅ (Hf ₅ Sc [*])	-7
	HfIr ₃ (L1 ₂)	HfIr ₃ (L1 ₂)	-800	Ru	-	Ir ₈ Ru(Pt ₈ Ti)	-20
Ti		Ir ₇ Ti(CuPt ₇)	-369			Ir ₃ Ru(L1 ₂)	-34
	Ir ₃ Ti(L1 ₂)	Ir ₃ Ti(L1 ₂)	-716			IrRu(B19)	-49
		Ir ₂ Ti(Ga ₂ Hf)	-779			IrRu ₂ (Ir ₂ Tc [*])	-54
		Ir ₅ Ti ₃ (Ga ₃ Pt ₅)	-809			IrRu ₃ (D0 ₁₉)	-53
	IrTi (Unkn.)	IrTi(L1 ₀)	-847		IrRu ₅ (Hf ₅ Sc [*])	-37	
	IrTi ₂ (C11 _b)	-712	Co	-	-		
	IrTi ₃ (A15)	IrTi ₃ (A15)	-566	Ir	Reference		
Nb	Ir ₃ Nb(L1 ₂)	Ir ₃ Nb(Co ₃ V)	-628(9)	Rh	-	Ir ₃ Rh(fcc ^[113] _{AB3})	-15
	IrNb(L1 ₀ / IrTa)	IrNb(L1 ₀)	-542(2)			Ir ₂ Rh(Pd ₂ Ti)	-20
	Ir _{0.37} Nb _{0.63} (σ)	Ir ₂ Nb ₅ (σ_{ABAB})	-484			IrRh(fcc ^[113] _{A2B2})	-21
	IrNb ₃ (A15)	IrNb ₃ (A15)	-433			IrRh ₂ (Pd ₂ Ti)	-18
Ta	Ir ₃ Ta(L1 ₂)	Ir ₃ Ta(Co ₃ V)	-688(2)	Ni	-	IrNi(NbP)	-38
		Ir ₂ Ta(Ga ₂ Hf)	-659	Pt	-	-	
	IrTa(L1 ₀ / IrTa)	IrTa(L1 ₀)	-594(3)	Pd	-	-	
	Ir _{0.25} Ta _{0.75} (σ)	Ir ₁₀ Ta ₂₀ (σ_{ABAB})	-528	Au	-	-	
		IrTa ₃ (A15)	-479	Ag	-	-	
V	Ir ₃ V(L1 ₂)	Ir ₃ V(D0 ₁₉)	-505(21)	Cu	-	-	
	IrV(IrV / L1 ₀)	IrV(L1 ₀)	-500 [§]	Hg	-	-	
	IrV ₃ (A15)	IrV ₃ (A15)	-497	Cd	-	-	
		IrV ₈ (Pt ₈ Ti)	-225	Zn		IrZn(IrZn [†])	-195
Mo	Ir ₃ Mo(D0 ₁₉)	Ir ₃ Mo(D0 ₁₉)	-332			IrZn ₂ (C49)	-238
		Ir ₂ Mo(C37)	-337			IrZn ₃ (NbPd ₃)	-224
	IrMo(B19)	IrMo(B19)	-321		Ir ₂ Zn ₁₁ (Ir ₂ Zn ₁₁)	Ir ₂ Zn ₁₁ (Ir ₂ Zn ₁₁)	-192
	IrMo ₃ (A15)		(75)				

TABLE IV: Compounds in **Rhodium** binary alloys. All symbols are as in Table III.

	Compounds		ΔH meV/at.		Compounds		ΔH meV/at.
	Exper.[35, 36]	Calc.			Exper.[35, 36]	Calc.	
Y	Rh ₃ Y(CeNi ₃)	Rh ₃ Y(CeNi ₃)	-569	W	Rh _{0.8} W _{0.2} (Mg)	Rh ₈ W(Pt ₈ Ti)	-140
	Rh ₂ Y(C15)	Rh ₂ Y(C15)	-742		Rh ₃ W(D0 ₁₉)	Rh ₃ W(D0 ₁₉)	-274
	RhY(B2)	RhY(B2)	-863			Rh ₂ W(C37)	-264
	Rh ₂ Y ₃ (Rh ₂ Y ₃)		$\langle 8 \rangle$	Cr	Cr ₃ Rh(A15)		$\langle 103 \rangle$
	Rh ₃ Y ₅ (Unkn.)	Rh ₃ Y ₅ (Pu ₅ Rh ₃)	-727			CrRh ₂ (C37)	-117
	Rh ₃ Y ₇ (Fe ₃ Th ₇)	Rh ₃ Y ₇ (Fe ₃ Th ₇)	-606		CrRh ₃ (L1 ₂)	CrRh ₃ (L1 ₂)	-128
	RhY ₃ (D0 ₁₁)	RhY ₃ (D0 ₁₁)	-517			CrRh ₇ (CuPt ₇)	-65
Sc		Rh ₇ Sc(CuPt ₇)	-348	Tc	-	Rh ₂ Tc(Ir ₂ Tc [*])	-157
	Rh ₃ Sc(L1 ₂)	Rh ₃ Sc(L1 ₂)	-620			RhTc(B19)	-175
	RhSc(B2)	RhSc(B2)	-1035			RhTc ₃ (D0 ₁₉)	-158
		Ir ₄ Sc ₁₁ (Ir ₄ Sc ₁₁)	-582	Re	-	Re ₃ Rh(D0 ₁₉)	-163
	Rh ₁₃ Sc ₅₇ (Rh ₁₃ Sc ₅₇)	Rh ₁₃ Sc ₅₇ (Rh ₁₃ Sc ₅₇)	-424			ReRh(B19)	-184
	Ir ₇ Sc ₄₄ (Mg ₄₄ Rh ₇)	-319		ReRh ₂ (Ir ₂ Tc [*])	-173		
Zr	Rh ₃ Zr(L1 ₂)	Rh ₃ Zr(L1 ₂)	-687	Mn	Mn ₃ Rh(L1 ₂)		$\langle 153 \rangle$
	Rh ₅ Zr ₃ (Pu ₃ Pd ₅)	Rh ₅ Zr ₃ (Pu ₃ Pd ₅)	-811		MnRh(B2)	MnRh(B2)	-190
	Rh ₄ Zr ₃ (Unkn.)					MnRh ₃ (L1 ₂)	-126
	RhZr(NiTi)	RhZr(B33)	-790 $\langle 3 \rangle$	Fe		MnRh ₇ (CuPt ₇)	-66
	RhZr ₂ (NiTi ₂ / C16)	RhZr ₂ (C11 _b)	-568 $\langle 34, 11 \rangle$			Fe ₃ Rh(bcc _{AB3} ^[001])	-49
	RhZr ₃ (D0 _e)	IrZr ₃ (SV ₃)	-428 [§]		Fe ₂ Rh(Fe ₂ Rh [†])	-57	
Hf	Hf ₂ Rh(NiTi ₂)	Hf ₂ Rh(CuZr ₂)	-633 $\langle 13 \rangle$		FeRh(B2)		$\langle 1 \rangle$
	HfRh(B2)	HfRh(B27)	-898 $\langle 29 \rangle$			FeRh ₃ (D0 ₂₄)	-56
	Hf ₃ Rh ₄ (Unkn.)			Os	-	OsRh(RhRu [*])	-8
	Hf ₃ Rh ₅ (Ge ₃ Rh ₅)	Hf ₃ Rh ₅ (Ge ₃ Rh ₅)	-928	Ru	-	Rh ₈ Ru(Pt ₈ Ti)	-2
	HfRh ₃ (L1 ₂)	HfRh ₃ (L1 ₂)	-762			RhRu(RhRu [*])	-8
Ti		Rh ₇ Ti(CuPt ₇)	-330			RhRu ₂ (RhRu ₂ [*])	-6
	Rh ₅ Ti(Unkn.)					RhRu ₅ (RhRu ₅ [*])	-3
	Rh ₃ Ti(L1 ₂)	Rh ₃ Ti(L1 ₂)	-631	Co	-	-	
	Rh ₅ Ti ₃ (Ge ₃ Rh ₅)	Rh ₅ Ti ₃ (Ge ₃ Rh ₅)	-790	Ir	-	Ir ₃ Rh(fcc _{AB3} ^[113])	-15
	RhTi(Unkn.)	RhTi(L1 ₀)	-749			Ir ₂ Rh(Pd ₂ Ti)	-20
	RhTi ₂ (CuZr ₂)	RhTi ₂ (C11 _b)	-629 $\langle 1 \rangle$		IrRh(fcc _{A2B2} ^[113])	-21	
Nb		Nb ₈ Rh(Pt ₈ Ti)	-131		IrRh ₂ (Pd ₂ Ti)	-18	
	Nb ₃ Rh(A15)	Nb ₃ Rh(A15)	-288	Rh	reference		
	Nb _{0.7} Rh _{0.3} (σ)	Nb ₂₀ Rh ₁₀ (σ_{BAABA})	-342	Ni	-	-	
	NbRh(L1 ₀ / IrTa)	NbTh(L1 ₀)	-436 $\langle 4 \rangle$	Pt	-	PtRh(NbP)	-25
	NbRh ₃ (L1 ₂ / Co ₃ V)	NbRh ₃ (Co ₃ V)	-548 $\langle 6 \rangle$			PtRh ₂ (Pd ₂ Ti)	-21
Ta	Rh ₃ Ta(L1 ₂)	Rh ₃ Ta(L1 ₂)	-611			PtRh ₃ (D0 ₂₂)	-18
	Rh ₂ Ta(C37)	Rh ₂ Ta(Ga ₂ Hf)	-597 $\langle 13 \rangle$	Pd	-	-	
	RhTa(IrTa)		$\langle 11 \rangle$	Au	-	-	
	Rh _{0.3} Ta _{0.7} (σ)	RhTa ₃ (A15)	-333	Ag	-	-	
		RhTa ₅ (RuTc ₅ [*])	-233	Cu	-	Cu ₇ Rh(CuPt ₇)	-4
	RhTa ₈ (Pt ₈ Ti)	-159	Hg	"Hg ₅ Rh"	Hg ₄ Rh(Hg ₄ Pt)	-40	
V		Rh ₅ V(HfPd ₅ [*])	-268				
	Rh ₃ V(L1 ₂)	Rh ₃ V(D0 ₁₉)	-393 $\langle 11 \rangle$		"Hg _{4.63} Rh"		
	RhV(IrV / L1 ₀)	RhV(L1 ₀)	-371 [§]		Hg ₂ Rh(Hg ₂ Pt)	$\langle 28 \rangle$	
	RhV ₃ (A15)	RhV ₃ (A15)	-332	Cd	"Cd ₂₁ Rh ₅ "	Cd ₄ Rh(Hg ₄ Pt)	-104
		RhV ₅ (RuTc ₅ [*])	-246			(γ -brass)	Cd ₂ Rh(Hg ₂ Pt)
	RhV ₈ (Pt ₈ Ti)	-170	Zn	"Rh ₅ Zn ₂₁ "	RhZn(B2)	-391	
Mo	MoRh(B19)	MoRh(B19)	-196		(γ -brass)	Rh ₃ Zn ₅ (Ga ₃ Pt ₅)	-395
		MoRh ₂ (C37)	-247			RhZn ₂ (ZrSi ₂)	-388
	MoRh ₃ (D0 ₁₉)	MoRh ₃ (D0 ₁₉)	-248			RhZn ₃ (D0 ₂₃)	-351
		MoRh ₈ (Pt ₈ Ti)	-116				

TABLE V: Compounds in **Platinum** binary alloys. tet-L1₂ denotes a tetragonal distortion of the L1₂ structure. All symbols are as in Table III.

	Compounds			ΔH meV/at.		Compounds			ΔH meV/at.		
	Exper.[35, 36]	Calc.				Exper.[35, 36]	Calc.				
Y	Pt ₅ Y (Unkn.)	Pt ₅ Y(D2 _d)		-677	Tc	-	Pt ₃ Tc(bcc _{AB3} ^[001])		-158		
	Pt ₃ Y(L1 ₂)	Pt ₃ Y(L1 ₂)		-983			Pt ₂ Tc(Ir ₂ Tc*)		-184		
	Pt ₂ Y(C15)	Pt ₂ Y(C15)		-1095			PtTc ₃ (D0 ₁₉)		-267		
	Pt ₄ Y ₃ (Unkn.)				Re	Pt ₃ Re(Unkn.)	Pt ₃ Re(bcc _{AB3} ^[001])		-128		
	PtY(B27)	PtY(B33)		-1252(54)				PtRe ₃ (D0 ₁₉)		-231	
	Pt ₄ Y ₅ (Ge ₄ Sm ₅)			(1)	Mn	Mn ₃ Pt(L1 ₂)	Mn ₃ Pt(D0 ₁₉)		-174(144)		
	Pt ₃ Y ₅ (Mn ₅ Si ₃)			(28)					MnPt(L1 ₀)		(293)
	PtY ₂ (Cl ₂ Pb)	PtY ₂ (Cl ₂ Pb)		-936				Mn ₃ Pt ₅ (Ga ₃ Pt ₅)		-363	
	Pt ₃ Y ₇ (Fe ₃ Th ₇)			(19)				MnPt ₂ (Ga ₂ Hf)		-365	
	PtY ₃ (D0 ₁₁)	PtY ₃ (D0 ₁₁)		-709			MnPt ₃ (L1 ₂)		MnPt ₃ (L1 ₂)	-363	
Sc		Pt ₈ Sc(Pt ₈ Ti)		-482	Fe	Fe ₃ Pt(L1 ₂)	FePt(L1 ₀)		(39)		
	Pt ₃ Sc(L1 ₂)	Pt ₃ Sc(L1 ₂)		-1050					FePt(L1 ₀)		-244
		Pt ₂ Sc(Ga ₂ Hf)		-1143					FePt ₂ (Ga ₂ Hf)		-220
	PtSc(B2)	PtSc(B2)		-1232			FePt ₃ (L1 ₂)	FePt ₃ (tet-L1 ₂ c/a=.992)		-203	
	PtSc ₂ (Cl ₂ Pb)	PtSc ₂ (Cl ₂ Pb)		-982				FePt ₅ (HfPd ₅ [‡])		-162	
		Pt ₁₃ Sc ₅₇ (Rh ₁₃ Sc ₅₇)	Pt ₁₃ Sc ₅₇ (Rh ₁₃ Sc ₅₇)			-571	Os	-	-		
Zr	Pt ₈ Zr(Pt ₈ Ti)	Pt ₈ Zr(Pt ₈ Ti)		-496	Ru	-	PtRu(CdTi)		-33		
	Pt ₃ Zr(D0 ₂₄ / L1 ₂)	Pt ₃ Zr(D0 ₂₄)		-1031(12)	Co	Co ₃ Pt(D0 ₁₉)	Co ₃ Pt(D0 ₁₉)		-97		
	Pt ₂ Zr(C11 _b)			(62)					CoPt(L1 ₀)		(12)
	Pt ₁₁ Zr ₉ (Pt ₁₁ Zr ₉)			(73)				CoPt ₂ (CuZr ₂)		-106	
	PtZr(T11)	PtZr(B33)		-1087(1)		CoPt ₃ (L1 ₂)		CoPt ₅ (HfPd ₅ [‡])	(16)		
	Pt ₃ Zr ₅ (D8 ₈)			(25)	Ir	-	-				
PtZr ₂ (NiTi ₂)	PtZr ₂ (C16)		-759(51)								
Hf	Hf ₂ Pt(NiTi ₂)	Hf ₂ Pt(NiTi ₂)		-786	Rh	-	PtRh(NbP)		-25		
	HfPt(B2/B33/T11)	HfPt(B33/T11)		-1155(165)				PtRh ₂ (Pd ₂ Ti)		-21	
	HfPt ₃ (L1 ₂ /D0 ₂₄)	HfPt ₃ (D0 ₂₄)		-1100(3)				PtRh ₃ (D0 ₂₂)		-18	
		HfPt ₈ (Pt ₈ Ti)		-528			Ni	Ni ₃ Pt (Unkn.)	Ni ₃ Pt(D0 ₂₂)		-76
					NiPt(L1 ₀)					-99	
					NiPt ₂ (CuZr ₂)					-75	
Ti							NiPt ₃ (D0 ₂₃)		-61		
	Pt ₈ Ti(Pt ₈ Ti)	Pt ₈ Ti(Pt ₈ Ti)		-433	Pt	reference					
		Pt ₅ Ti(HfPd ₅ [‡])		-617		Pd	-	Pd ₇ Pt(CuPt ₇)		-14	
	Pt ₃ Ti(D0 ₂₄ /L1 ₂)	Pt ₃ Ti(PuAl ₃)		-864(3, 5)					Pd ₃ Pt(CdPt ₃ [‡])		-25
		Pt ₂ Ti(C49)		-912					PdPt(L1 ₁)		-36
		Pt ₃ Ti ₂ (Pd ₃ Ti ₂)		-931					PdPt ₃ (L1 ₂)		-26
	PtTi(B19)	PtTi(NiTi)		-933(5)					PdPt ₇ (CuPt ₇)		-15
	PtTi ₃ (A15)	PtTi ₃ (A15)		-648	Au			-	-		
Nb	Nb ₃ Pt(A15)	Nb ₃ Pt(A15)		-415	Ag	Ag ₃ Pt(L1 ₂)	Ag ₇ Pt(CuPt ₇)		-13		
	Nb _{0.6} Pt _{0.4} (σ)							Ag ₃ Pt ₂ (Ag ₃ Pt ₂ [‡])		-38	
	NbPt(B19)	NbPt(L1 ₀)		-660(13)				AgPt(Unkn.)	AgPt(L1 ₁)		-39
	NbPt ₂ (MoPt ₂)	NbPt ₂ (MoPt ₂)		-721				AgPt ₃ (Unkn.)			
	NbPt ₃ (L6 ₀ /NbPt ₃)	NbPt ₃ (NbPt ₃ /D0 _a)		-678(154)			Cu	Cu ₇ Pt(CuPt ₇)	Cu ₇ Pt(CuPt ₇)		-87
	NbPt ₈ (Pt ₈ Ti)		-378		Cu ₃ Pt(L1 ₂)	Cu ₃ Pt(L1 ₂)			-143		
					CuPt(L1 ₁)	CuPt(L1 ₁)			-166		
Ta		Pt ₈ Ta(Pt ₈ Ti)		-416		Cu ₃ Pt ₅ (Unkn.)					
	Pt ₃ Ta(D0 ₂₂ /L6 ₀ /NbPt ₃)	Pt ₃ Ta(NbPt ₃)		-723(11, 183)		CuPt ₃ (Unkn.)	CuPt ₃ (CdPt ₃ [‡])		-121		
	Pt ₂ Ta(Au ₂ V)	Pt ₂ Ta(Au ₂ V)		-757		CuPt ₇ (CuPt ₇)	CuPt ₇ (CuPt ₇)		-77		
		PtTa(L1 ₀)		-643							
	Pt _{0.25} Ta _{0.75} (σ)	Pt ₈ Ta ₂₂ (σ BBBAB)		-434	Hg	Hg ₄ Pt(Hg ₄ Pt)	Hg ₄ Pt(Hg ₄ Pt)		-104		
Pt _{0.6} Ta _{3.74} (A15)	PtTa ₃ (A15)		-416			Hg ₂ Pt(Hg ₂ Pt)		(25)			
	PtTa ₈ (Pt ₈ Ti)		-197			HgPt ₃ (Unkn.)					
V		Pt ₈ V(Pt ₈ Ti)		-275	Cd	Cd ₅ Pt(Cd ₅ Pt-partial occupancy)					
	Pt ₃ V(D0 ₂₂)	Pt ₃ V(D0 _a)		-464(4)			Cd ₄ Pt(Hg ₄ Pt)		-228		
	Pt ₂ V(MoPt ₂)	Pt ₂ V(MoPt ₂)		-555			Cd ₃ Pt (Unkn.)	Cd ₃ Pt(D0 ₁₁)		-260	
	PtV(B19)	PtV(L1 ₀)		-563(2)			Cd ₇ Pt ₃ (Unkn.)				
PtV ₃ (A15)	PtV ₃ (A15)		-436		Cd ₂ Pt(Unkn.)	Cd ₂ Pt(Hg ₂ Pt)		-316			
	PtV ₈ (Pt ₈ Ti)		-206		CdPt(L1 ₀)	CdPt(L1 ₀)		-322			
Mo		MoPt ₈ (Pt ₈ Ti)		-202		CdPt ₃ (L1 ₂)	CdPt ₃ (CdPt ₃ [‡])		-190(11)		
	Mo ₃ Pt(D0 ₁₉)			(38)	Zn	Pt ₇ Hg(CuPt ₇)		-189			
	MoPt(B19)	MoPt(B19)		-321			Pt ₃ Zn(L1 ₂)	Pt ₃ Zn(CdPt ₃ [‡])		-331(6)	
	MoPt ₂ (MoPt ₂)	MoPt ₂ (MoPt ₂)		-366			PtZn(L1 ₀)	PtZn(L1 ₀)		-570	
MoPt ₃ (Unkn.)						PtZn ₂ (C49)	PtZn ₂ (C49)		-463		
		MoPt ₄ (D1 _a)		-265		PtZn ₃ (D0 ₂₂)	PtZn ₃ (D0 ₂₂)		-397		
		MoPt ₈ (Pt ₈ Ti)		-180		Pt ₂ Zn ₁₁ (Ir ₂ Zn ₁₁)		-272			
W		Pt ₄ W(D1 _a)		-270							
	Pt ₂ W(MoPt ₂)	Pt ₂ W(MoPt ₂)		-343							
	PtW (Unkn.)										
Cr	Cr ₃ Pt(A15 / L1 ₂)			(70)							
	CrPt(L1 ₀)	CrPt(B19)		-191(31)							
	CrPt ₃ (L1 ₂)	CrPt ₃ (L1 ₂)		-261							
		CrPt ₈ (Pt ₈ Ti)		-136							

TABLE VI: Compounds in **Palladium** binary alloys. tet-fcc denotes a tetragonal distortion of stacked fcc superstructures. All symbols are as in Table III.

	Compounds		ΔH meV/at.		Compounds		ΔH meV/at.	
	Exper.[35, 36]	Calc.			Exper.[35, 36]	Calc.		
Y	Pd ₇ Y(CuPt ₇)	Pd ₇ Y(CuPt ₇)	-442	Re	-	PdRe ₃ (D0 ₁₉)	-56	
	Pd ₃ Y(L1 ₂)	Pd ₃ Y(L1 ₂)	-863	Mn	MnPd(L1 ₀)	(5)		
	Pd ₂ Y (Unkn.)			Mn ₃ Pd ₅ (Ga ₃ Pt ₅)	Mn ₃ Pd ₅ (Ga ₃ Pt ₅)	-250		
	Pd ₃ Y ₂ (Unkn.)				MnPd ₂ (C37)	-252		
	Pd ₄ Y ₃ (Pd ₄ Pu ₃)	Pd ₄ Y ₃ (Pd ₄ Pu ₃)	-923		MnPd ₃ (L1 ₂)	-234(10)		
	PdY (Unkn.)	PdY(B33)	-913		MnPd ₅ (HfPd ₅ [‡])	-175		
	Pd ₂ Y ₃ (Ni ₂ Er ₃)		(8)		MnPd ₈ (Pt ₈ Ti)	-125		
		PdY ₂ (C37)	-622	Fe	Fe _{0.96} Pd _{1.04} (L1 ₀)	(22)		
					FePd ₂ (CuZr ₂)	-116		
		PdY ₃ (D0 ₁₁)	PdY ₃ (D0 ₁₁)	-475		FePd ₃ (D0 ₂₃)	-112(2)	
Sc		Pd ₈ Sc(Pt ₈ Ti)	-411		FePd ₅ (HfPd ₅ [‡])	-100		
	Pd ₃ Sc(L1 ₂)	Pd ₃ Sc(L1 ₂)	-855		FePd ₈ (Pt ₈ Ti)	-81		
	Pd ₂ Sc (Unkn.)	Pd ₂ Sc(C37)	-898	Os	-	-		
	PdSc(B2)	PdSc(B2)	-906	Ru	-	-		
	PdSc ₂ (NiTi ₂)	PdSc ₂ (NiTi ₂)	-660	Co	-	CoPd ₃ (tet-fcc ^[001] _{AB3} c/a=2.8)	-10	
	PdSc ₄ (Unkn.)			Ir	-	-		
Zr		Pd ₈ Zr(Pt ₈ Ti)	-424	Rh	-	-		
		Pd ₅ Zr(HfPd ₅ [‡])	-591	Ni	-	NiPd ₃ (tet-fcc ^[001] _{AB3} c/a=2.7)	-6	
	Pd ₃ Zr(D0 ₂₄)	Pd ₃ Zr(D0 ₂₄)	-816	Pt	-	Pd ₇ Pt(CuPt ₇)	-14	
	Pd ₂ Zr(C11 _b)		(1)		Pd ₃ Pt(CdPt ₃ [‡])	-25		
	Pd ₄ Zr ₃ (Pd ₄ Pu ₃)		(2)		PdPt(L1 ₁)	-36		
	PdZr (Unkn.)	PdZr(B33)	-645		PdPt ₃ (L1 ₂)	-26		
	Pd ₃ Zr ₅ (D8 ₈)		(90)		PdPt ₇ (CuPt ₇)	-15		
	PdZr ₂ (NiTi ₂ / CuZr ₂)	PdZr ₂ (C11 _b /CuZr ₂)	-487(83)	Pd	reference			
	Hf	Hf ₂ Pd(C11 _b / CuZr ₂)	Hf ₂ Pd(C11 _b /CuZr ₂)	-527	Au		Au ₅ Pd(HfPd ₅ [‡])	-55
		HfPd (Unkn.)	HfPd(B33)	-685		Au ₃ Pd(Unkn.)	Au ₃ Pd(D0 ₂₃)	-82
		Hf ₂ Pd ₃ (Pd ₃ Ti ₂)	-778			Au ₂ Pd(C49)	-88	
Hf ₃ Pd ₄ (Unkn.)					AuPd (Unkn.)	AuPd(NbP)	-94	
		Hf ₃ Pd ₅ (Pd ₅ Ti ₃)	-800		AuPd ₃ (Unkn.)	AuPd ₃ (L1 ₂)	-56	
HfPd ₂ (C11 _b)			(9)	Ag	-	Ag ₇ Pd(CuPt ₇)	-33	
HfPd ₃ (D0 ₂₄ /L1 ₂)		HfPd ₃ (D0 ₂₄)	-879(11)			Ag ₅ Pd(HfPd ₅ [‡])	-41	
Ti		HfPd ₅ (HfPd ₅ [‡])	-635			Ag ₃ Pd(D0 ₂₃)	-58	
		HfPd ₈ (Pt ₈ Ti)	-430			Ag ₂ Pd(C37)	-63	
						Ag ₂ Pd ₃ (Ag ₂ Pd ₃ [‡])	-63	
	Pd _{3.2} Ti _{0.8} (L1 ₂)		(7)			AgPd(L1 ₁)	-59	
	Pd ₃ Ti(D0 ₂₄)	Pd ₃ Ti(D0 ₂₄)	-646			AgPd ₃ (CdPt ₃ [‡])	-31	
	Pd ₂ Ti(Pd ₂ Ti)	Pd ₂ Ti(Pd ₂ Ti)	-632	Cu	Cu ₇ Pd(CuPt ₇)	(18)		
	Pd ₅ Ti ₃ (Pd ₅ Ti ₃)	Pd ₅ Ti ₃ (Pd ₅ Ti ₃)	-615			Cu ₅ Pd(HfPd ₅ [‡])	-72	
	Pd ₃ Ti ₂ (Pd ₃ Ti ₂)	Pd ₃ Ti ₂ (Pd ₃ Ti ₂)	-602		Cu ₃ Pd(L1 ₂ / SrPb ₃)	Cu ₃ Pd(D0 ₂₃)	-107(2, 5)	
	PdTi(B19)		(5)			Cu ₂ Pd(Ga ₂ Hf)	-117	
	PdTi ₂ (CuZr ₂)	PdTi ₂ (C11 _b /CuZr ₂)	-451		CuPd (Unkn.)	CuPd(B2)	-125	
Pd _{0.8} Ti _{3.2} (A15)	PdTi ₃ (A15)	-342			CuPd ₃ (L1 ₂)	-71		
Nb		Nb ₃ Pd(Nb ₃ Pd [‡])	-167		CuPd ₇ (CuPt ₇)	CuPd ₇ (CuPt ₇)	-37	
		Nb ₂ Pd(CuZr ₂)	-220	Hg	Hg ₄ Pd(Unkn.)	Hg ₄ Pd(Hg ₄ Pt)	-101	
	Nb _{0.6} Pd _{0.4} (σ)					(65)		
	NbPd ₂ (MoPt ₂)	NbPd ₂ (MoPt ₂)	-432		Hg ₅ Pd ₂ (Hg ₅ Mn ₂)	Hg ₂ Pd(Hg ₂ Pt)	-150	
	NbPd ₃ (NbPd ₃ / D0 ₂₂)	NbPd ₃ (NbPd ₃)	-435(2)			HgPd(L1 ₀)	-174	
		NbPd ₅ (HfPd ₅ [‡])	-356			Hg ₃ Pd ₅ (Ga ₃ Pt ₅)	-166	
Ta		NbPd ₈ (Pt ₈ Ti)	-279			HgPd ₂ (C37)	-160	
	Pd ₈ Ta(Pt ₈ Ti)	Pd ₈ Ta(Pt ₈ Ti)	-325					
	Pd ₅ Ta(HfPd ₅ [‡])	Pd ₅ Ta(HfPd ₅ [‡])	-401		HgPd ₃ (Unkn.)	HgPd ₃ (D0 ₂₂)	-139	
	Pd ₃ Ta(D0 ₂₂)	Pd ₃ Ta(D0 ₂₂)	-480			HgPd ₄ (D1 _a)	-112	
	Pd ₂ Ta(MoPt ₂)	Pd ₂ Ta(MoPt ₂)	-458	Cd	Cd ₁₁ Pd ₂ (Ir ₂ Zn ₁₁)	Cd ₁₁ Pd ₂ (Ir ₂ Zn ₁₁)	-171	
PdTa(B11)	PdTa(B11)	-362		Cd ₄ Pd (Unkn.)				
Pd _{0.25} Ta _{0.75} (σ)				Cd ₃ Pd (Unkn.)				
	PdTa ₈ (Pt ₈ Ti)	-98			Cd ₂ Pd(Hg ₂ Pt)	-307		
V		Pd ₈ V(Pt ₈ Ti)	-177			CdPd(L1 ₀)	-418(164)	
						CdPd ₂ (C37)	-334	
	Pd ₃ V(D0 ₂₂)	Pd ₃ V(NbPd ₃)	-253(6)		CdPd(CuTi)	CdPd ₂ (C37)	-334	
	Pd ₂ V(MoPt ₂)	Pd ₂ V(MoPt ₂)	-274			CdPd ₃ (D0 ₂₂)	-272	
	PdV (Unkn.)		(9)			CdPd ₄ (D1 _a)	-225	
	PdV ₃ (A15)					CdPd ₅ (HfPd ₅ [‡])	-188	
	Pd ₅ V(Mo ₅ Ti [*])	-115			CdPd ₇ (CuPt ₇)	-142		
	PdV ₈ (Pt ₈ Ti)	-94	Zn		Pd ₈ Zn(Pt ₈ Ti)	-165		
Mo	MoPd ₂ (MoPt ₂)	MoPd ₂ (MoPt ₂)	-99			Pd ₂ Zn(C37)	-462	
		MoPd ₄ (D1 _a)	-92			PdZn(L1 ₀)	-570(187)	
		MoPd ₈ (Pt ₈ Ti)	-86					
	Pd ₈ W(Pt ₈ Ti)	-122		Pd ₃ Zn ₅ (Unkn.)				
Cr	-					PdZn ₃ (D0 ₂₂)	-359	
	Cr _{0.49} Pd _{0.51} (In)	CrPd ₃ (L1 ₂)	-81			Pd ₂ Zn ₁₁ (Ir ₂ Zn ₁₁)	-243	
	Cr _{1.33} Pd _{2.67} (L1 ₂)	CrPd ₅ (HfPd ₅ [‡])	-76					
Tc	-	PdTc(RhRu [*])	-63					
		PdTc ₃ (D0 ₁₉)	-73					

TABLE VII: Geometry of new prototypes marked by † in tables III to VI.

Formula	IrZn	Nb ₃ Pd	Fe ₂ Rh	Ag ₃ Pt ₂	Ag ₂ Pd ₃
Lattice	Monoclinic	Orthorhombic	Orthorhombic	Rhombohedral	Monoclinic
Space Group	<i>C2/m</i> No. 12	<i>Cmmm</i> No. 65	<i>Cmmm</i> No. 65	<i>R3m</i> No. 166	<i>C2/m</i> No. 12
Pearson symbol	mS8	oS8	oS12	hR5	mS10
Bravais lattice type	MCLC	ORCC	ORCC	RHL	MCLC
Lattice variation [44]	MCLC ₁	ORCC	ORCC	RHL ₁	MCLC ₃
Conv. Cell: <i>a, b, c</i> (Å)	1.94, 3.83, 1.12	1.26, 1.78, 3.56	1.78, 5.35, 1.26	1.12, 1.12, 13.75	3.55, 1.59, 1.94
α, β, γ (deg)	72.98, 90, 90	90, 90, 90	90, 90, 90	90, 90, 120	65.9, 90, 90
Wyckoff positions [45]	Ir $\frac{1}{6}, \frac{1}{2}, -0.292$ (4i) Zn $\frac{1}{6}, \frac{1}{2}, -0.208$ (4i)	Nb1 0, 0, $\frac{1}{4}$ (4k) Nb2 $\frac{1}{2}, 0, \frac{1}{2}$ (2c) Pd $\frac{1}{2}, 0, 0$ (2b)	Fe1 $\frac{1}{6}, 0, 0$ (4g) Fe2 0, 0, $\frac{1}{2}$ (2d) Fe3 $\frac{1}{2}, 0, 0$ (2b) Rh $\frac{1}{3}, 0, \frac{1}{2}$ (4h)	Ag1 0, 0, $\frac{1}{5}$ (2c) Ag2 0, 0, 0 (1a) Pt 0, 0, $\frac{2}{5}$ (2c)	Ag $\frac{3}{10}, \frac{1}{2}, \frac{1}{10}$ w (4i) Pd1 0, 0, $\frac{1}{2}$ (2c) Pd2 $\frac{1}{10}, \frac{1}{2}, \frac{7}{10}$ (4i)
AFLOW label [33]	123	72	b83	f38	f55

[48], Miedema formation enthalpy [49], Zunger pseudo-potential radii maps [50], and Pettifor maps [42, 43]. These empirical rules and structure maps have helped direct a few successful searches for previously unobserved compounds [51]. However, they offer a limited response to the challenge of identifying new compounds because they rely on the existence of consistent and reliable experimental input for systems spanning most of the relevant parameter space. In many cases, reliable information is missing in a large portion of this space, e.g. less than 50% of the binary systems have been satisfactorily characterized [52]. This leaves considerable gaps in the empirical structure maps and reduces their predictive usefulness. The advance of HT computational methods makes it possible to fill these gaps in the experimental data with complementary *ab initio* data by efficiently covering extensive lists of candidate structure types [28]. This development was envisioned by Pettifor a decade ago [51], and here we present its realization for PGM alloys.

Fig. 2 shows a Pettifor structure map, enhanced by our HT computational results, for structures of 1:1 stoichiometry. The elements along the map axes are ordered according to Pettifor’s chemical scale (χ parameter) [43]. Circles indicate agreement between computation and experiment, regarding the existence of 1:1 compounds, or lack thereof. If the circle contains a label (Strukturbericht or prototype) this denotes the structure that is stable in the given system at this stoichiometry. Rectangles denote disagreement between experiments and computation about the 1:1 compounds, in systems reported as compound forming (blue rectangles) or as non-compound forming (red and gray rectangles). In the lower left part of the map, there is a region of non-compound forming systems, whereas the upper part of the map is mostly composed of compound-forming systems. In the upper part of the map, experiment and computation agree, preserving a large cluster of B2 structures, or differ slightly on the structure reported to have the lowest formation enthalpy at 1:1 (blue rectangles). For example, the 1:1 phases of Hf-Pd and Pd-Zr are unknown according to the phase diagram literature, but we find the stable phases with B33 structure, right next to Hf-Pt in the diagram, which is reported as a B33 structure. Similarly, stable L1₀ structures are identified in the Ir-Ti and Rh-Ti systems, adjacent to a reported cluster of this

structure. Two additional L1₀ structures are identified in the Cd-Pd and Pd-Zn systems, instead of the reported CuTi structures, extending a small known cluster of this structure at the bottom right corner of the map. These are examples of the capability of HT *ab initio* results to complement the empirical Pettifor maps, and extend their regions of predictive input, in a way consistent with the experimental data.

In the middle of the map, in a rough transition zone between compound-forming and non-compound-forming regions, computation finds quite a few cases where stable compounds are predicted in systems where none have been reported experimentally (pink rectangles). Most prominent here is a large cluster of B19 compounds. Nine systems marked by light gray rectangles are reported in experiments as having no compounds, but our calculations find stable compounds at stoichiometries other than 1:1.

At the stoichiometries of 1:2 and 2:1, Fig. 3 shows significant additions of the calculations to the experimental data on compound-formation. Again, the systems where computation finds stable compounds in experimentally non-compound-forming systems are found at the border between the compound-forming region (dark gray circles and white labeled circles) and the non-compound-forming region (light gray circles), or fill isolated gaps within the compound-forming regions. The calculations augment islands of structurally-similar regions, yielding a more consistent structure map. For example, calculation finds the CuZr₂ structure for Nb-Pd, extending the island of this structure already present in the experimental results (left panel, upper right). The calculations significantly extend the Hg₂Pt island in the lower right of the B₂A panel, from a single experimental entry to 6 systems (in Hg-Pt itself, the calculation finds this structure slightly unstable at $T = 0K$, 25meV/atom above the stability tie-line). A cluster of σ phases in the left panel shows that this reported disordered phase has underlying ordered realizations at low temperatures. Three completely new islands, for the C37, Ga₂Hf and IrTc₂ structures, appear near the upper center of the A₂B panel. Another new cluster, of the Pd₂Ti structure, appears at the lower center of both panels. In general, the clusters of blue rectangles, show that the calculations augment the experimental results in a consistent manner.

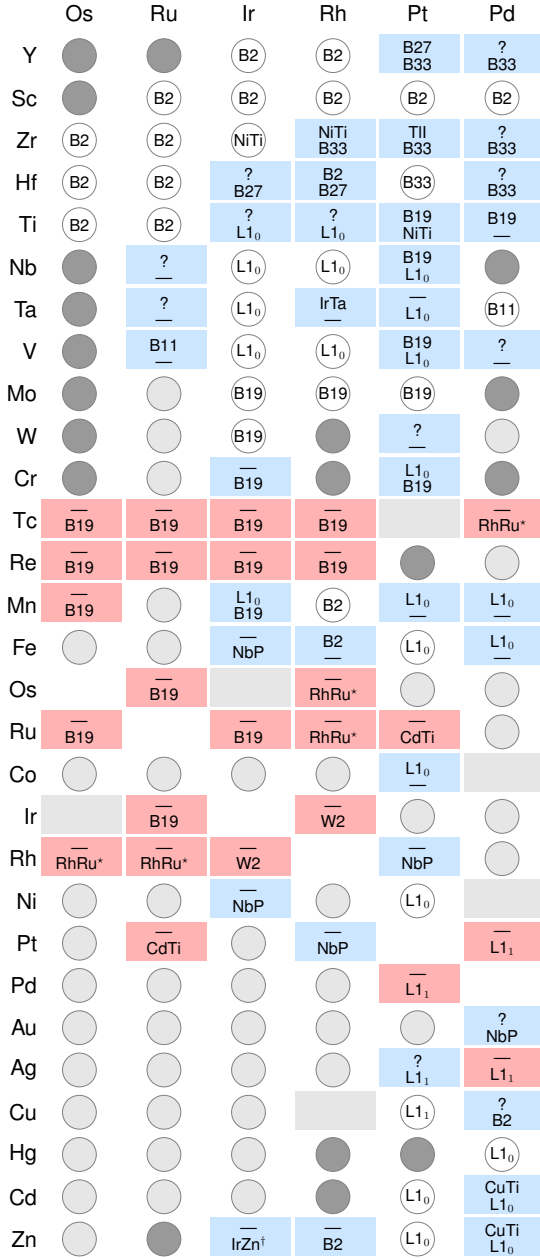


FIG. 2: A Pettifor-type structure map for 1:1 stoichiometry compounds in PGM binary systems. Circles indicate agreement between experiment and computation: white circles with Strukturbericht or prototype labels denote 1:1 compounds, dark circles indicate a compound-forming system with no compounds at 1:1, light circles denote non-compound forming systems. Blue rectangles denote compound-forming systems where the reported and computed stable structures differ at 1:1 stoichiometry. The top label in the rectangle is the reported structure, the bottom label is the structure we find to be stable in this work. A dash “—” indicates the absence of a stable structure. Unidentified suspected structures are denoted by a question mark “?”. Pink rectangles indicate systems reported as non-compound forming, with a dash at the top of the rectangle, but we find a stable 1:1 phase, identified at the bottom of the rectangle. Light gray rectangles indicate systems reported as non-compound forming where a structure is predicted at a stoichiometry different from 1:1. A dark gray rectangle indicates a system reported with a disordered compound where no stable structures are found in the calculation.

The structure map for 1:3 phases is shown in Fig. 4. Similarly to the 1:1 and 1:2 maps, the calculation extends structural islands of the experimental data, most new phases in non-compound-forming systems occur in systems at the boundary between compound-forming and non-compound-forming regions, and there is significant agreement between the experimentally reported phases (or lack thereof) and calculated phases. In the upper part of the right panel, the L₁₂ and D₀₂₄ clusters are preserved with slight modifications at their boundaries (at Pt-Ti, the PuAl₃ structure is only 3 meV/atom lower than the experimental structure D₀₂₄, a difference too small to be significant). The D₀₁₉ cluster is significantly expanded. In the left panel, the calculations introduce a new D₀₁₉ island near the center of the diagram. New small regions of the D₀₂₂ structures emerge at the right bottom of both panels. Adjacent D₀₂₃ and CdPt₃* islands appear in the left and right panels, respectively. The experimental D_{0e} structure for RhZr₃ may actually be SV₃, since in the calculation the D_{0e} structure relaxed into the SV₃ structure, creating a small SV₃ island at the top of the left panel.

The structure maps of figs. 2 to 4 give a bird’s eye view of the exhaustive HT search for new structures. Consistently with the empirical maps, they show significant separation of different structures into regions where the constituent elements have a similar Pettifor χ number. The HT data significantly enhances the empirical maps, extends the regions of some structures, fills in apparent gaps and indicates previously unsuspected structure clusters. Moreover, the HT data contains more detail than is apparent in the structure maps. Even when calculation and experiment agree that a system is compound-forming (green [dark gray] circles in Fig. 1), the calculations often find additional stable compounds, beyond those known in experiment. When the reported structures are found to be unstable in the calculation, they are usually just slightly less stable than the calculated groundstate, or just slightly above the convex hull in a two phase region. Such cases and numerous additional predictions of marginally stable structures harbor further opportunities for materials engineering and applications.

V. CONCLUSIONS

In this study, the low temperature phase diagrams of all binary PGM-transition metal systems are constructed by HT *ab initio* calculations. The picture of PGM alloys emerging from this study is much more complete than that depicted by current experimental data, with dozens of stable structures that have not been previously reported. We predict ordering in 37 systems reported to be phase-separating and in five systems where only disordered phases are reported. In addition, in the known ordering systems, we find many cases in which more phases are predicted to be stable than reported in the experimental phase diagrams. These *ab initio* results complement the ordering tendencies implied by the empirical Pettifor maps. Augmenting the experimental data compiled in the phase-diagram databases [35, 36] with high-throughput

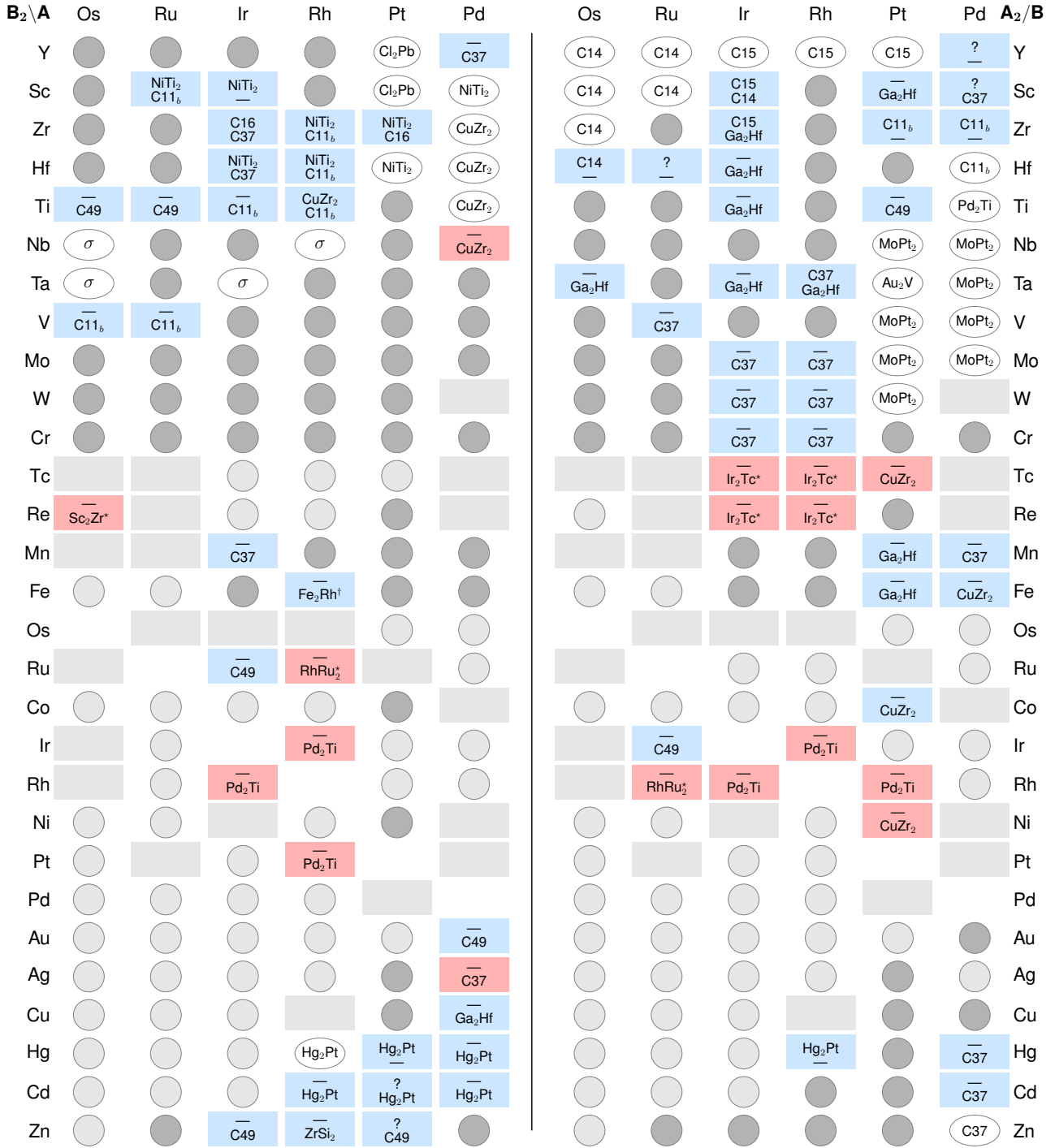


FIG. 3: A Pettifor-type structure map for 1:2 stoichiometry compounds in PGM binary systems. The symbols are as in Fig. 2, with the map stoichiometry changed respectively from 1:1 to 1:2 or 2:1.

first-principles data [33, 34], we construct Pettifor-type structure maps that point to new opportunities for alloys research. These maps demonstrate that the integration of the empirical and computational data produces enhanced maps that should provide a more comprehensive foundation for rational materials design. The theoretical predictions presented here will hopefully serve as a motivation for their experimental validation and be a guide for future studies of these important systems.

The maps in Figs. 2-4 include a large number of light blue rectangles, pointing to experiment-theory mismatches on structures at simple compositions in binary systems known to be compound forming. This may raise reservations that the level of theory employed, DFT-PBE, may not be as good as commonly accepted for transition metal alloys. A more careful look, however, shows that many of these mismatches, e.g. HfIr, PdZr, Cd₂Pt, CuPt₃ and Au₃Pd, involve cases where a compound of unknown struc-

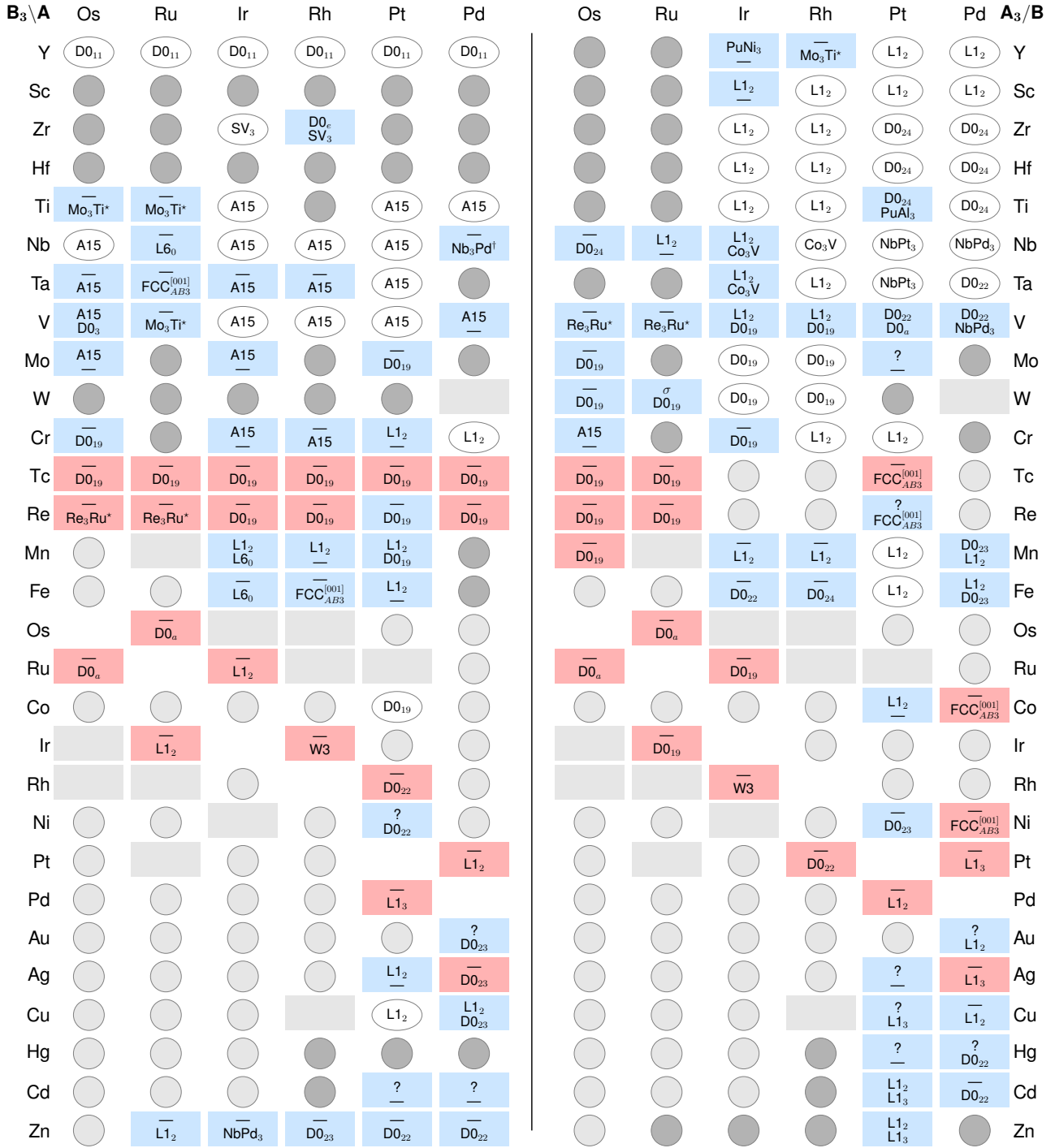


FIG. 4: A Pettifor-type structure map for 1:3 stoichiometry compounds in PGM binary systems. The symbols are as in Fig. 2.

ture has been reported by experiments. The calculation thus reveals the stable structure and closes the gap in the experimental data. In most other cases, e.g. RhZr, PtV, Ir₃V, Rh₂Ta, Cu₃Pt, the energy difference between the reported structure and the calculated structure or two-phase tie-line is rather small and is congruent with the adjacent structure clusters in the maps. Similar improved consistency with reported structure clusters also appears in cases where the discrepancies are considerable, e.g. CdPd and PdZn. In addition, as discussed in Sec. III, the calcula-

tions reproduce many complex large unit cell structures that are reported in the experimental literature. Moreover, it is important to remember that experiments are performed at room temperature or higher, while our calculations are carried out at zero temperature. Many phase discrepancies may therefore be due to vibrational promotion [53], or the tendency of structures to gain symmetries by loosing their internal Peierls instabilities or Jahn-Teller distortions. Therefore, the disagreements emerging in our calculations may not be a sign of deficiencies in the theo-

retical treatment, but a demonstration of its usefulness is bridging gaps in the experimental data and extending it towards unknown phase transitions at lower temperatures. The ultimate test of this issue rests with experimental validation of at least some of our predictions, which would hopefully be motivated by this work.

To help accelerate this process of experimental validation, discovery and development of materials [54] we are in the process of setting up a public domain REST-API that will allow the scientific community to download information from the www.aflowlib.org repository. It would ultimately enable researchers to generate alloy information remotely on their own personal computers. Extension of the database to nano-alloys and nano-sintered systems is planned within the size-pressure approximation (i.e. Fig.2 of Ref. [55]), to study trends of solubility and size-dependent disorder-order transitions and segregation in nano-catalysts [21, 55–57], and nano-crystals [58, 59].

A few of our predictions correspond to phases where the driving force for ordering is small (i.e., the formation enthalpy is small and it may be difficult to reach thermal equilibrium), however, it should be noted that some experimentally reported phases have similarly small formation enthalpies. Some of these predicted phases could be more easily realized as nano-structured phases, where the thermodynamics for their formation may be more favorable. Our results should serve as the foundation for finite temperature simulations to identify phases that are kinetically accessible. Rapid thermodynamical modelling and descriptor-based screening of systems predicted to harbor new phases should be used to pinpoint those with the greatest potential for applications [28]. Such simulations would be an invaluable extension to this work, however, the necessary tools to accomplish them on a similarly large scale are not yet mature.

Acknowledgments

SC acknowledges support from DOD-ONR (N00014-13-1-0635, N00014-11-1-0136, N00014-09-1-0921). GLWH is grateful for support from the National Science Foundation, DMR-0908753. OL thanks the Center for Materials Genomics of Duke University for its hospitality. The authors thank Dr. K. Rasch and Dr. C. E. Calderon for useful comments.

Appendix

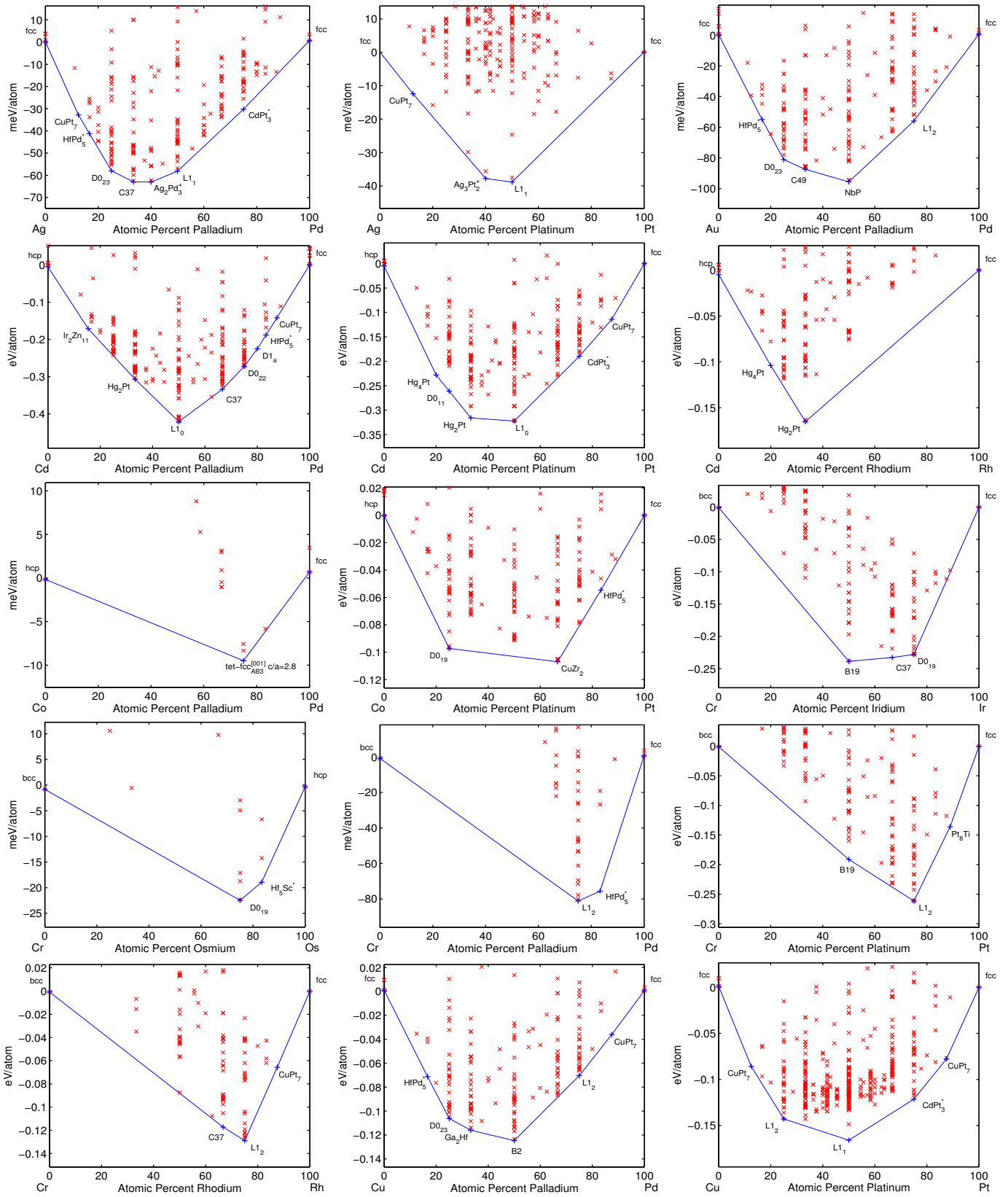


FIG. 5: Convex hulls for the systems AgPd, AgPt, AuPd, CdPd, CdPt, CdRh, CoPd, CoPt, CrIr, CrOs, CrPd, CrPt, CrRh, CuPd, and CuPt.

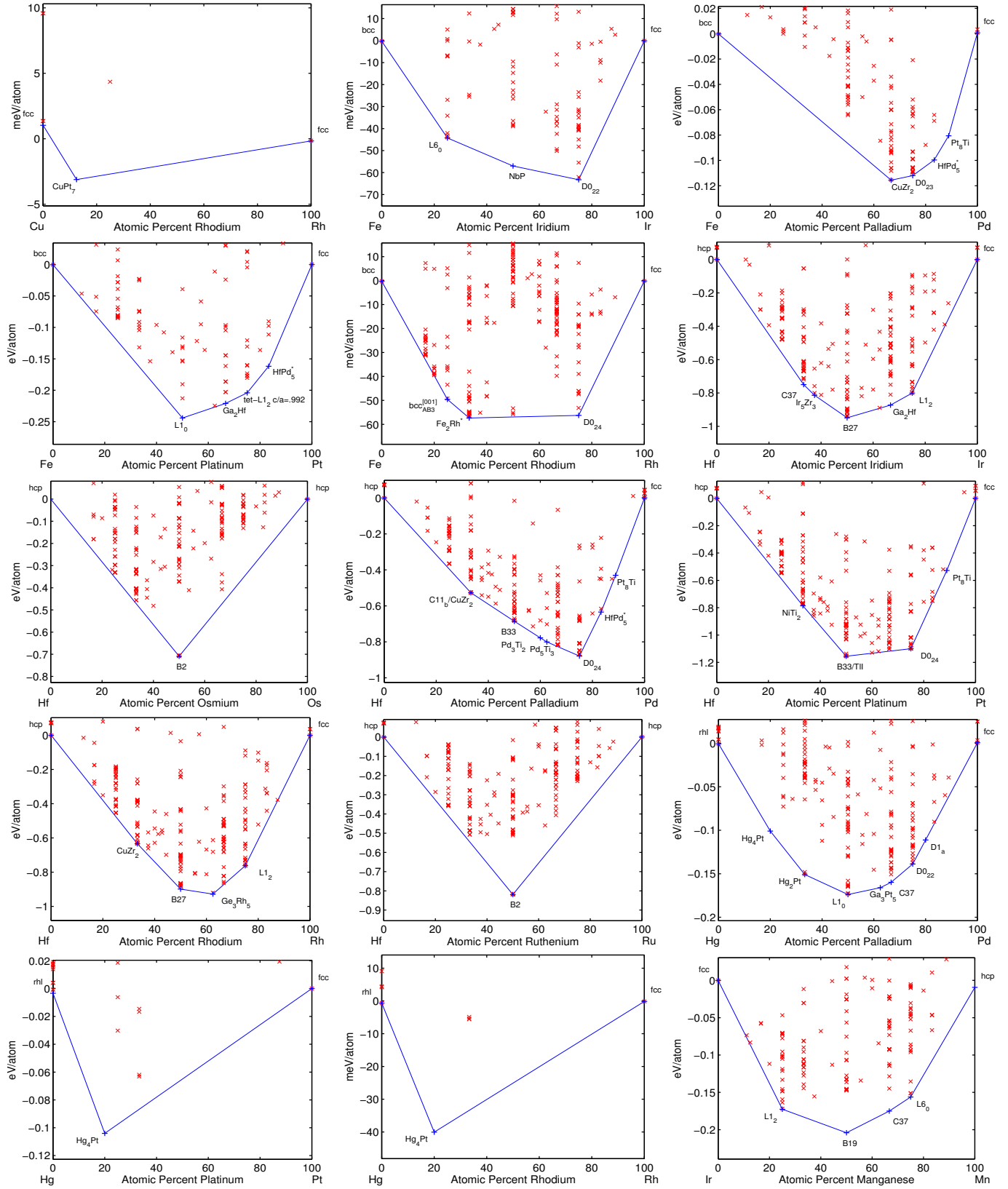


FIG. 6: Convex hulls for the systems CuRh, FeIr, FePd, FePt, FeRh, HfIr, HfOs, HfPd, HfPt, HfRh, HfRu, HgPd, HgPt, HgRh, and IrMn.

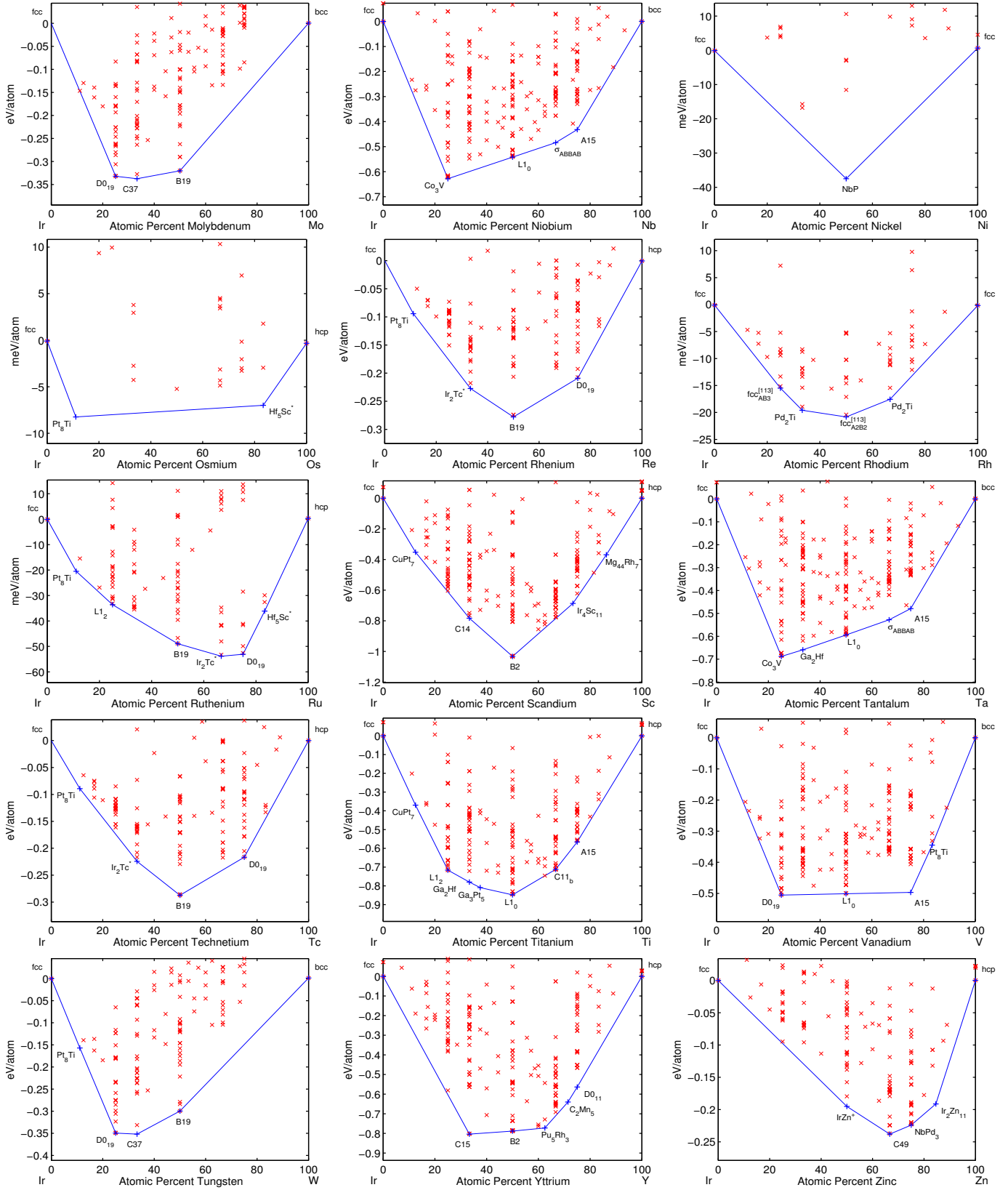


FIG. 7: Convex hulls for the systems IrMo, IrNb, IrNi, IrOs, IrRe, IrRh, IrRu, IrSc, IrTa, IrTc, IrTi, IrV, IrW, IrY, and IrZn.

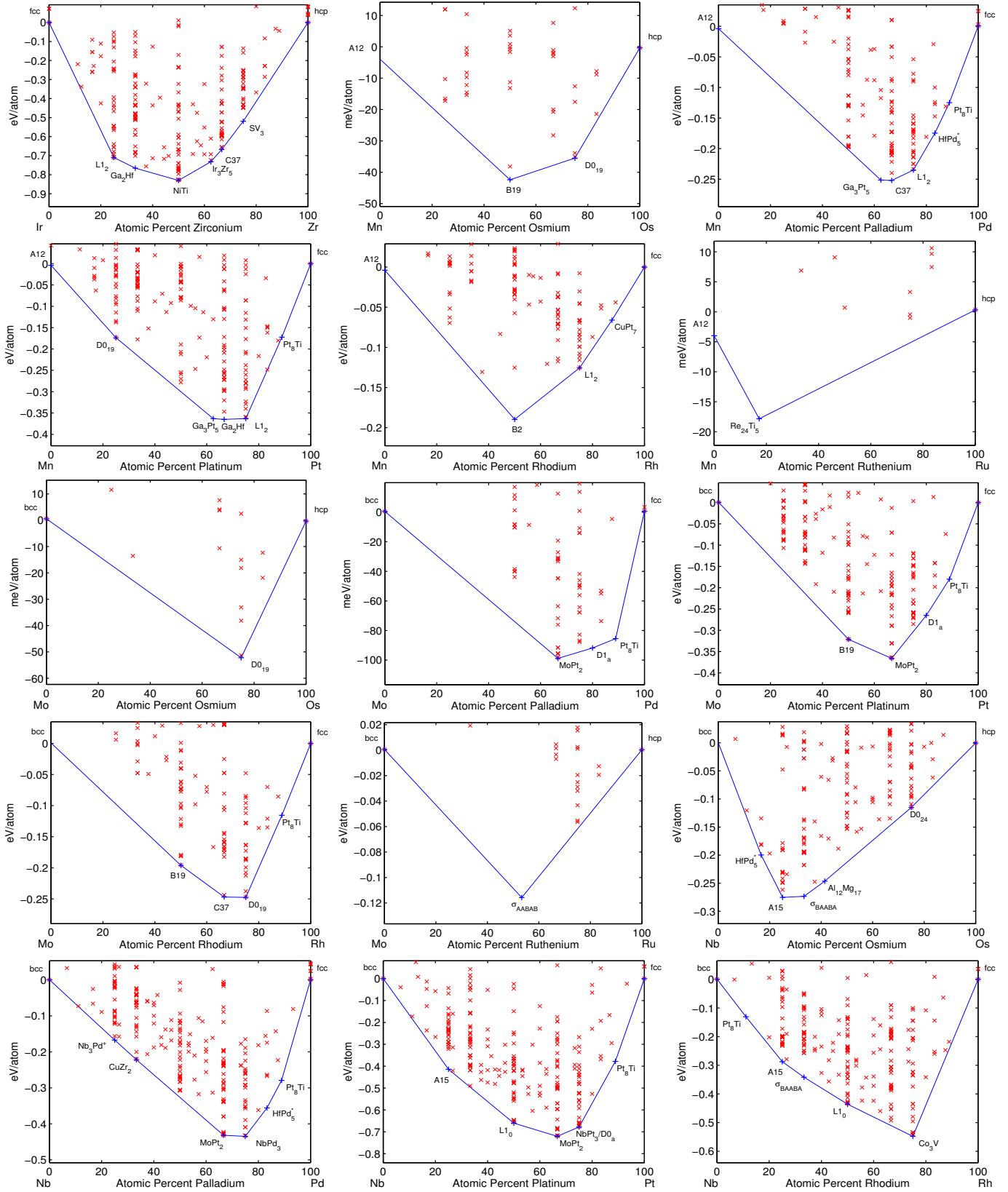


FIG. 8: Convex hulls for the systems IrZr, MnOs, MnPd, MnPt, MnRh, MnRu, MoOs, MoPd, MoPt, MoRh, MoRu, NbOs, NbPd, NbPt, and NbRh.

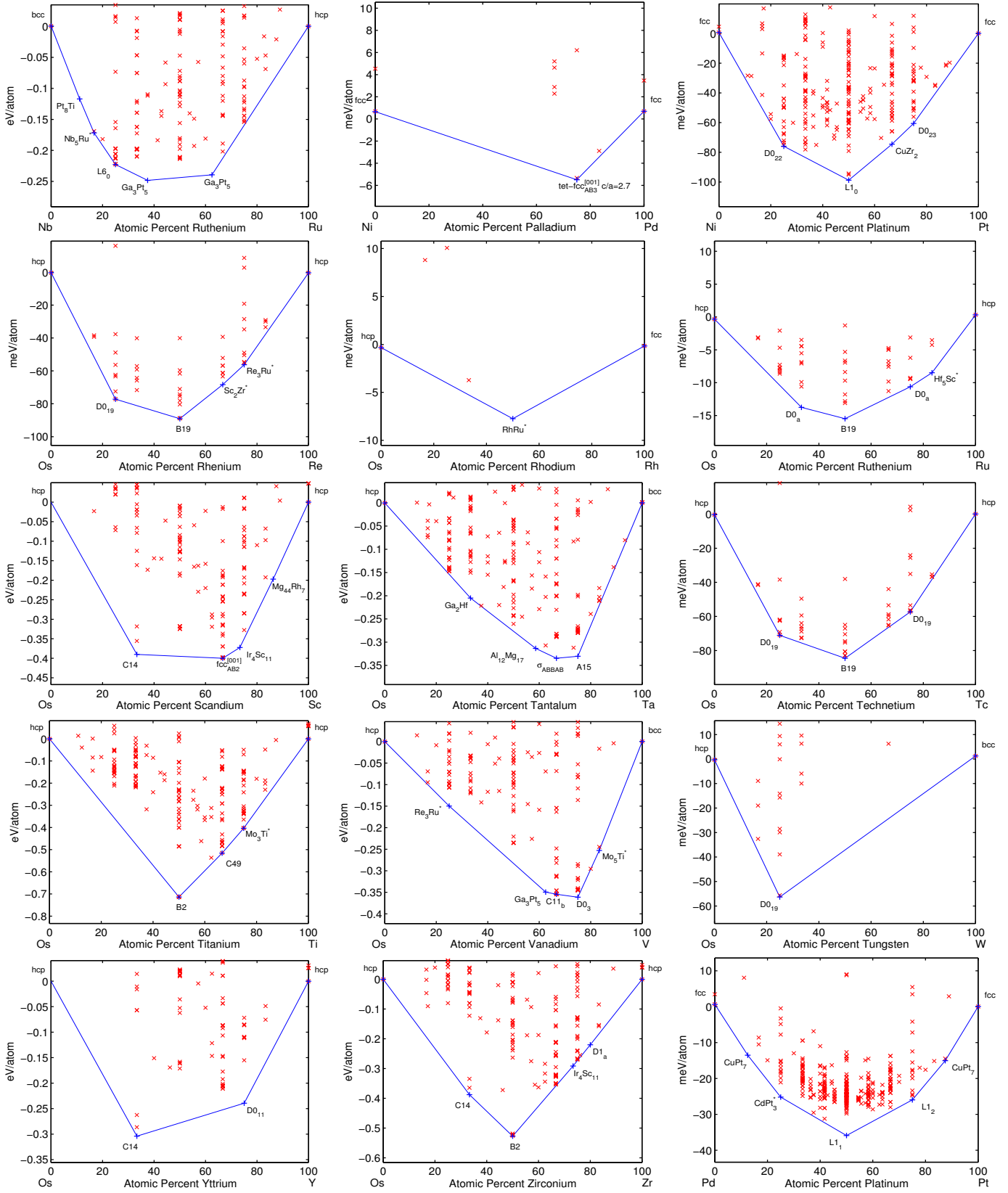


FIG. 9: Convex hulls for the systems NbRu, NiPd, NiPt, OsRe, OsRh, OsRu, OsSc, OsTa, OsTc, OsTi, OsV, OsW, OsY, OsZr, PdPt, and PdRe.

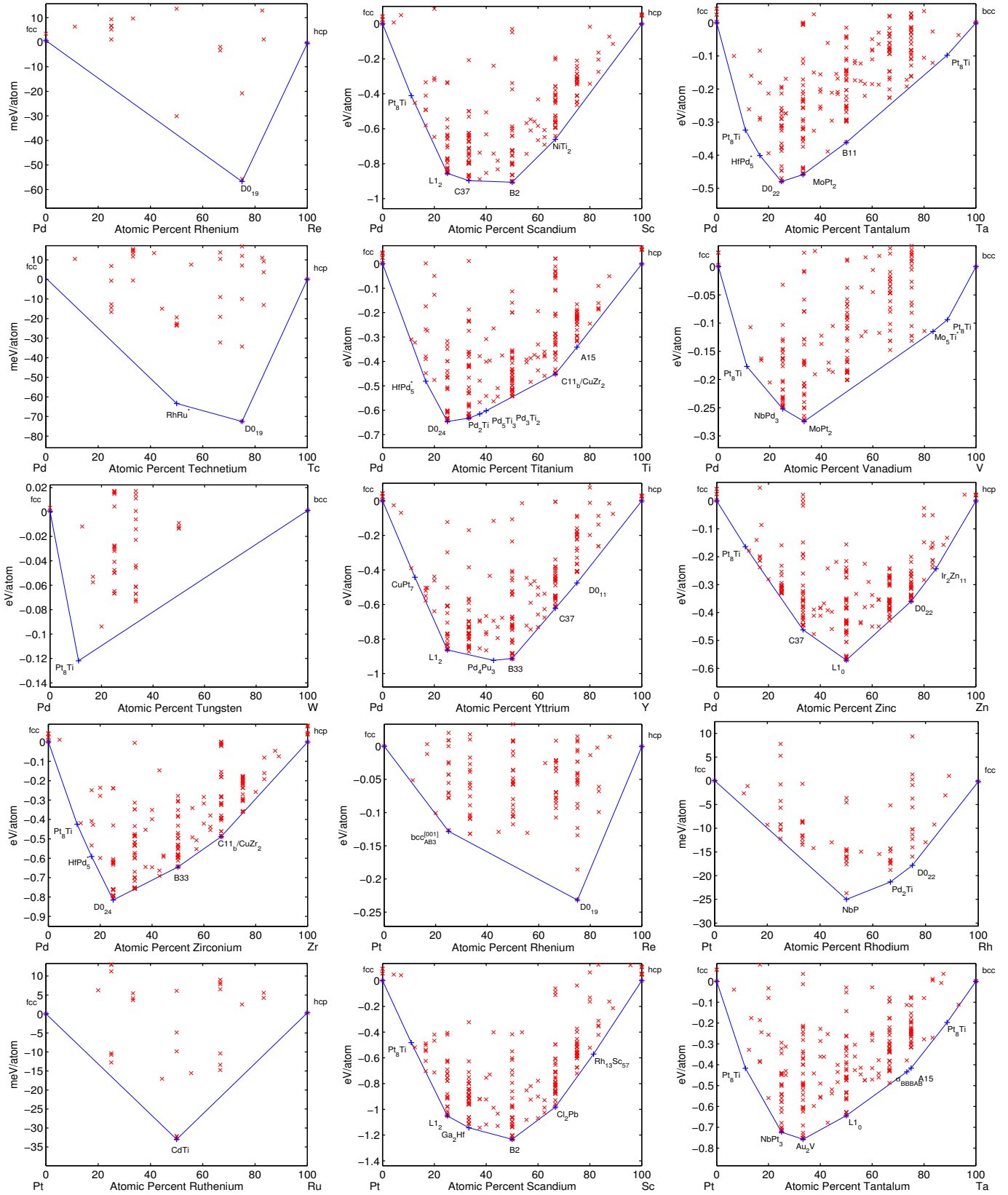


FIG. 10: Convex hulls for the systems PdSc, PdTa, PdTc, PdTi, PdV, PdW, PdY, PdZn, PdZr, PtRe, PtRh, PtRu, PtSc, PtTa, and PtTc.

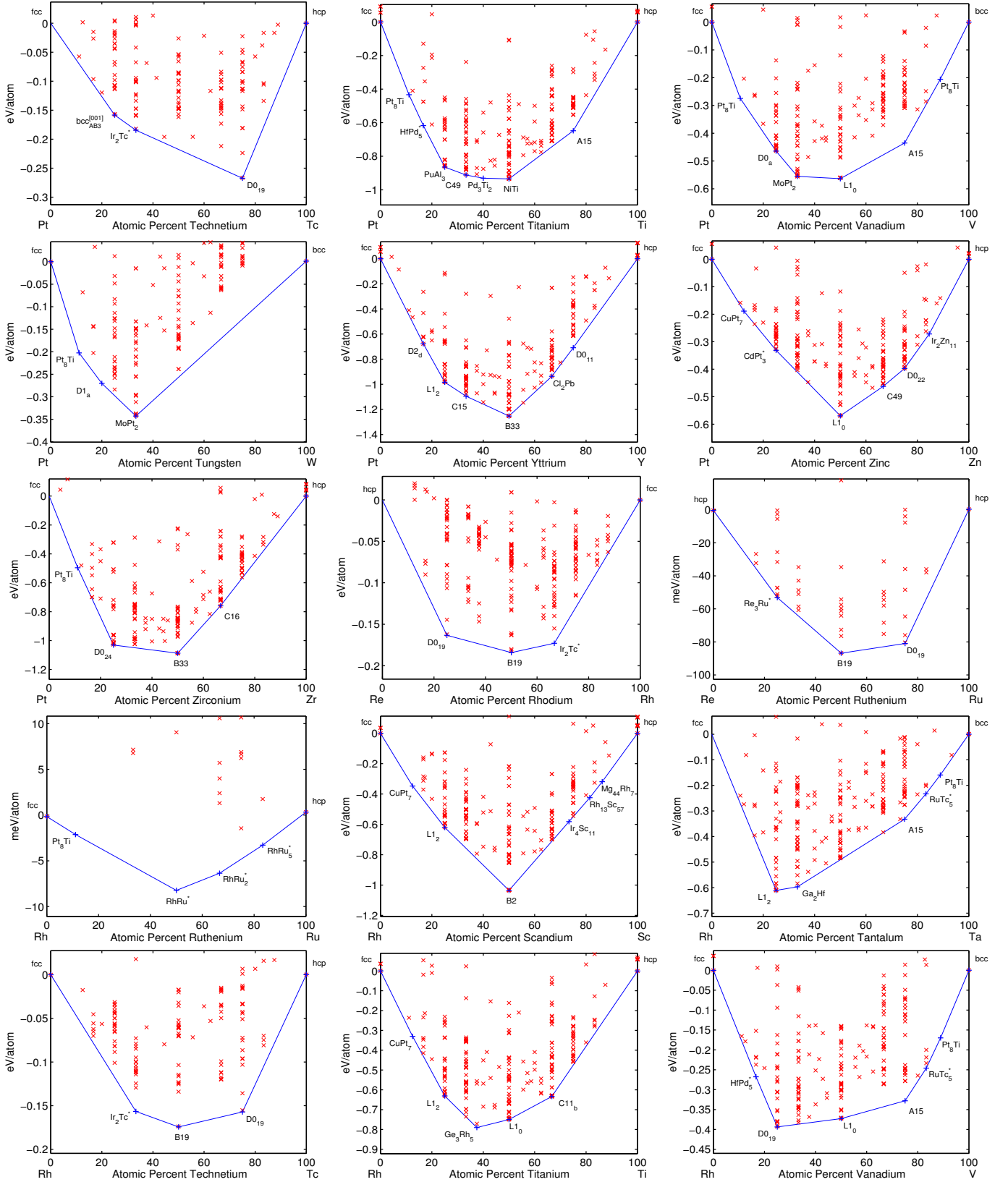


FIG. 11: Convex hulls for the systems PtTi, PtV, PtW, PtY, PtZn, PtZr, ReRh, ReRu, RhRu, RhSc, RhTa, RhTc, RhTi, RhV, and RhW.

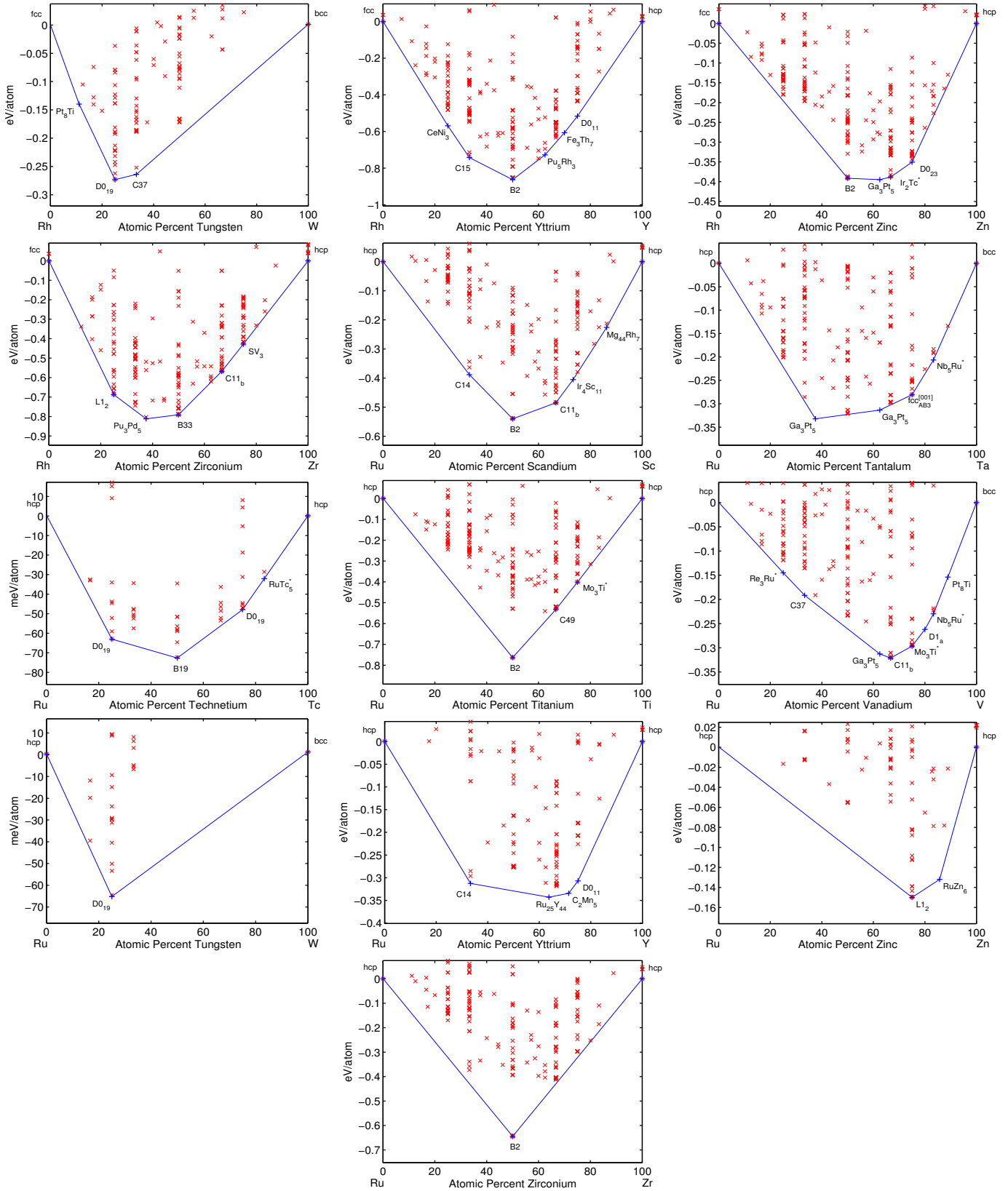


FIG. 12: Convex hulls for the systems RhY, RhZn, RhZr, RuSc, RuTa, RuTc, RuTi, RuV, RuW, RuY, RuZn, and RuZr.

-
- [1] P. J. Loferski, *2008 Minerals yearbook - Platinum Group Metals* (US Geological Survey, 2008).
- [2] S. Curtarolo, D. Morgan, and G. Ceder, *Accuracy of ab initio methods in predicting the crystal structures of metals: review of 80 binary alloys*, *Calphad* **29**, 163–211 (2005).
- [3] A. V. Ruban, I. A. Abrikosov, and H. L. Skriver, *Ground-state properties of ordered, partially ordered, and random Cu-Au and Ni-Pt alloys.*, *Phys. Rev. B* **51**, 12958–12968 (1995).
- [4] D. Paudyal and A. Mookerjee, *Phase stability and magnetism in NiPt and NiPd alloys*, *J. Phys.: Conden. Matt.* **16**, 5791–5802 (2004).
- [5] D. Paudyal, T. Saha-Dasgupta, and A. Mookerjee, *Phase stability-analysis in Fe-Pt and Co-Pt alloy systems: an augmented space study*, *J. Phys.: Conden. Matt.* **16**, 7247–7260 (2004).
- [6] D. Paudyal, T. Saha-Dasgupta, and A. Mookerjee, *Study of phase stability in NiPt systems*, *J. Phys.: Conden. Matt.* **15**, 1029–1046 (2003).
- [7] N. A. Zarkevich, T. L. Tan, and D. D. Johnson, *First-principles prediction of phase-segregating alloy phase diagrams and a rapid design estimate of their transition temperatures*, *Phys. Rev. B* **75**, 104203 (2007).
- [8] S. Bärthlein, E. Winning, G. L. W. Hart, and S. Müller, *Stability and instability of long-period superstructures in binary Cu-Pd alloys: A first-principles study*, *Acta Mater.* **57**, 1660–1665 (2009).
- [9] S. Bärthlein, G. L. W. Hart, A. Zunger, and S. Müller, *Reinterpreting the Cu-Pd phase diagram based on new ground-state predictions*, *J. Phys.: Conden. Matt.* **19**, 032201 (2007).
- [10] R. Taylor, S. Curtarolo, and G. L. W. Hart, *Predictions of the Pt₃Ti phase in unexpected systems*, *J. Am. Chem. Soc.* **132**, 6851 (2010).
- [11] M. J. Mehl, G. L. Hart, and S. Curtarolo, *Density functional study of the L1₀- α IrV transition in IrV and RhV*, *J. Alloys Compound.* **509**, 560–567 (2011).
- [12] R. V. Chepulskii and S. Curtarolo, *Revealing low-temperature atomic ordering in bulk Co-Pt with the high-throughput ab initio method*, *Appl. Phys. Lett.* **99**, 261902 (2011).
- [13] G. L. W. Hart, *Verifying predictions of the L1₃ crystal structure in Cd-Pt and Pd-Pt by exhaustive enumeration*, *Phys. Rev. B* **80**, 014106 (2009).
- [14] B. Schoenfeld, M. Engelke, and A. V. Ruban, *Lack of support for adaptive superstructure NiPt₇: Experiment and first-principles calculations*, *Phys. Rev. B* **79**, 064201 (2009).
- [15] K. Yuge, A. Seko, A. Kuwabara, F. Oba, and I. Tanaka, *First-principles study of bulk ordering and surface segregation in Pt-Rh binary alloys*, *Phys. Rev. B* **74**, 174202 (2006).
- [16] S. L. Shang, Y. Wang, D. E. Kim, C. L. Zacherl, Y. Du, and Z. K. Liu, *Structural, vibrational, and thermodynamic properties of ordered and disordered Ni_{1-x}Pt_x alloys from first-principles calculations*, *Phys. Rev. B* **83**, 144204 (2011).
- [17] D. A. Carr, J. Corbitt, G. R. Hart, E. Gilmartin, and G. L. W. Hart, *Finding new phases for precipitate-hardening in Platinum and Palladium alloys*, *Comp. Mat. Sci.* **51**, 331–339 (2012).
- [18] B. Sanyal, S. K. Bose, V. Drchal, and J. Kudrnovsky, *Ordering and segregation in XPt (X=V, Cu, and Au) random alloys*, *Phys. Rev. B* **64**, 134111 (2001).
- [19] P. E. A. Turchi, V. Drchal, and J. Kudrnovsky, *Stability and ordering properties of fcc alloys based on Rh, Ir, Pd, and Pt*, *Phys. Rev. B* **74**, 064202 (2006).
- [20] M. H. F. Sluiter, C. Colinet, and A. Pasturel, *Ab initio calculation of the phase stability in Au-Pd and Ag-Pt alloys*, *Phys. Rev. B* **73**, 174204 (2006).
- [21] R. V. Chepulskii, W. H. Butler, A. van de Walle, and S. Curtarolo, *Surface segregation in nanoparticles from first principles: the case of FePt*, *Scr. Mater.* **62**, 179–182 (2010).
- [22] L. J. Nelson, S. Curtarolo, and G. L. W. Hart, *Ground state characterizations of systems predicted to exhibit L1₁ or L1₃ crystal structures*, *Phys. Rev. B* **85**, 054203 (2012).
- [23] S. V. Barabash, V. Blum, S. Mueller, and A. Zunger, *Prediction of unusual stable ordered structures of Au-Pd alloys via a first-principles cluster expansion*, *Phys. Rev. B* **74**, 035108 (2006).
- [24] O. Levy, R. V. Chepulskii, G. L. W. Hart, and S. Curtarolo, *New face of Rhodium alloys: revealing ordered structures from first principles*, *J. Am. Chem. Soc.* **132**, 833–837 (2010).
- [25] M. Jahnatek, O. Levy, G. L. W. Hart, L. J. Nelson, R. V. Chepulskii, J. Xue, and S. Curtarolo, *Ordered Structures and Vibrational Stabilization in Ruthenium Alloys from First Principles Calculations*, *Phys. Rev. B* **84**, 214110 (2011).
- [26] O. Levy, G. L. W. Hart, and S. Curtarolo, *Uncovering compounds by synergy of cluster expansion and high-throughput methods*, *J. Am. Chem. Soc.* **132**, 4830–4833 (2010).
- [27] O. Levy, G. L. W. Hart, and S. Curtarolo, *Structure maps for hcp metals from first-principles calculations*, *Phys. Rev. B* **81**, 174106 (2010).
- [28] S. Curtarolo, G. L. W. Hart, M. Buongiorno Nardelli, N. Mingo, S. Sanvito, and O. Levy, *The high-throughput highway to computational materials design*, *Nat. Mater.* **12**, 191–201 (2013).
- [29] O. Levy, G. L. W. Hart, and S. Curtarolo, *Hafnium Binary Alloys from Experiments and First Principles*, *Acta Mater.* **58**, 2887–2897 (2010).
- [30] O. Levy, M. Jahnatek, R. V. Chepulskii, G. L. W. Hart, and S. Curtarolo, *Ordered Structures in Rhenium Binary Alloys from First-Principles Calculations*, *J. Am. Chem. Soc.* **133**, 158–163 (2011).
- [31] O. Levy, J. Xue, S. Wang, G. L. W. Hart, and S. Curtarolo, *Uncovering Technetium binary ordered structures from first principles*, *Phys. Rev. B* **85**, 012201 (2012).
- [32] A. R. Harutyunyan, E. Mora, T. Tokune, K. Bolton, A. Rosén, A. Jiang, N. Awasthi, and S. Curtarolo, *Hidden features of the catalyst nanoparticles favorable for single-walled carbon nanotube growth*, *Appl. Phys. Lett.* **90**, 163120 (2007).
- [33] S. Curtarolo, W. Setyawan, G. L. W. Hart, M. Jahnatek, R. V. Chepulskii, R. H. Taylor, S. Wang, J. Xue, K. Yang, O. Levy, M. Mehl, H. T. Stokes, D. O. Demchenko, and D. Morgan, *AFLOW: an automatic framework for high-throughput materials discovery*, *Comp. Mat. Sci.* **58**, 218–226 (2012).
- [34] S. Curtarolo, W. Setyawan, S. Wang, J. Xue, K. Yang, R. H. Taylor, L. J. Nelson, G. L. W. Hart, S. Sanvito, M. Buongiorno Nardelli, N. Mingo, and O. Levy, *AFLOWLIB.ORG: A distributed materials properties*

- repository from high-throughput *ab initio* calculations, *Comp. Mat. Sci.* **58**, 227–235 (2012).
- [35] P. Villars, M. Berndt, K. Brandenburg, K. Cenzual, J. Daams, F. Hulliger, T. Massalski, H. Okamoto, K. Osaki, A. Prince, H. Putz, and S. Iwata, *The Pauling File, Binaries Edition*, *J. Alloys Compound.* **367**, 293–297 (2004).
- [36] T. B. Massalski, H. Okamoto, P. R. Subramanian, and L. Kacprzak, eds., *Binary Alloy Phase Diagrams* (American Society for Metals, Materials Park, OH, 1990).
- [37] G. L. W. Hart and R. W. Forcade, *Generating derivative structures: Algorithm and applications*, *Phys. Rev. B* **77**, 224115 (2008).
- [38] G. Kresse and J. Hafner, *Ab initio molecular dynamics for liquid metals*, *Phys. Rev. B* **47**, 558–561 (1993).
- [39] P. E. Blöchl, *Projector augmented-wave method*, *Phys. Rev. B* **50**, 17953–17979 (1994).
- [40] J. P. Perdew, K. Burke, and M. Ernzerhof, *Generalized gradient approximation made simple*, *Phys. Rev. Lett.* **77**, 3865–3868 (1996).
- [41] H. J. Monkhorst and J. D. Pack, *Special points for Brillouin-zone integrations*, *Phys. Rev. B* **13**, 5188–5192 (1976).
- [42] D. G. Pettifor, *A chemical scale for crystal-structure maps*, *Sol. State Commun.* **51**, 31–34 (1984).
- [43] D. G. Pettifor, *The structures of binary compounds. I. Phenomenological structure maps*, *J. Phys. C: Solid State Phys.* **19**, 285–313 (1986).
- [44] W. Setyawan and S. Curtarolo, *High-throughput electronic band structure calculations: challenges and tools*, *Comp. Mat. Sci.* **49**, 299–312 (2010).
- [45] T. Hahn, ed., *International Tables of Crystallography. volume A: Space-group symmetry* (Kluwer Academic publishers, International Union of Crystallography, Chester, England, 2002).
- [46] J. K. Stalick, K. Wang, and R. M. Waterstrat, *The Crystal Structure and Phase Transition of Hf_2Pt_3* , *Journal of Phase Equilibria and Diffusion* (2013).
- [47] G. L. W. Hart and R. W. Forcade, *Generating derivative structures from multilattices: Application to hcp alloys*, *Phys. Rev. B* **80**, 014120 (2009).
- [48] W. Hume-Rothery, *The Metallic State* (Oxford University Press, Oxford, 1931).
- [49] A. R. Miedema, P. F. de Chatel, and F. R. de Boer, *Cohesion in alloys - fundamentals of a semi-empirical model*, *Physica B&C* **100B**, 1 (1980).
- [50] A. Zunger, *Systematization of the stable crystal structure of all AB-type binary compound: A pseudopotential orbital-radii approach*, *Phys. Rev. B* **22**, 5839 (1980).
- [51] D. G. Pettifor, *Structure maps revisited*, *J. Phys.: Condens. Matter.* **15**, V13–V16 (2003).
- [52] P. Villars, K. Brandenburg, M. Berndt, S. LeClair, A. Jackson, Y. H. Pao, B. Igel'nik, M. Oxley, B. Bakshi, P. Chen, and S. Iwata, *Binary, ternary and quaternary compound former/nonformer prediction via Mendeleev number*, *J. Alloys Compound.* **317-318**, 26–38 (2001).
- [53] C. Wolverton and V. Ozoliņš, *Entropically Favored Ordering: The Metallurgy of Al_2Cu Revisited*, *Phys. Rev. Lett.* **86**, 5518 (2001).
- [54] Editorial, *Fuelling discovery by sharing*, *Nat. Mater.* **12**, 173 (2013).
- [55] A. R. Harutyunyan, N. Awasthi, A. Jiang, W. Setyawan, E. Mora, T. Tokune, K. Bolton, and S. Curtarolo, *Reduced carbon solubility in Fe nano-clusters and implications for the growth of single-walled carbon nanotubes*, *Phys. Rev. Lett.* **100**, 195502 (2008).
- [56] S. Curtarolo, N. Awasthi, W. Setyawan, A. Jiang, K. Bolton, T. Tokune, and A. R. Harutyunyan, *Influence of Mo on the Fe:Mo:C nano-catalyst thermodynamics for single-walled carbon nanotube growth*, *Phys. Rev. B* **78**, 054105 (2008).
- [57] F. Cervantes-Sodi, T. P. McNicholas, J. G. S. Jr., J. Liu, G. Csányi, A. C. Ferrari, and S. Curtarolo, *Viscous State Effect on the Activity of Fe Nano-catalysts*, *ACS Nano* **4**, 6950–6956 (2010).
- [58] T. Chookajorn, H. A. Murdoch, and C. A. Schuh, *Design of Stable Nanocrystalline Alloys*, *Science* **337**, 951–954 (2012).
- [59] H. A. Murdoch and C. A. Schuh, *Stability of binary nanocrystalline alloys against grain growth and phase separation*, *Acta Mater.* **61**, 2121–2132 (2013).